NTNU – Trondheim
Norwegian University of
Science and Technology

Contacts to P-doped GaAs Nanowires by Fabrication of Electrodes using Metals and Graphene

Ole Morten Christoffersen

Master of Science in Electronics
Submission date: June 2012
Supervisor: Helge Weman, IET

Norwegian University of Science and Technology
Department of Electronics and Telecommunications

Abstract

P-type GaAs semiconducting nanowires (NWs) with NW/electrode contacts have been examined by fabricating single NW devices to investigate their electrical properties. Both NWs grown with Au-assisted and Ga-assisted vapor-liquid-solid (VLS) method have been examined, with great emphasis on Ga-assisted NWs because these show superior contact properties. The NWs were grown using molecular beam epitaxy (MBE) and electrical contacts were fabricated using electron beam litography, electron beam evaporation for metallization and annealing to enhance ohmic behaviour of the contacts. Two different types of contacts were tested. One was metal contacts where various combinations of metal layers were tested, including such metallizations as Pt/Ti/Pt/Au and Pd/Zn/Pd/Au. The second electrode type was graphene which is expected to show very interesting electric and opto-electronic properties.

It is shown in this thesis that ohmic contact with linear I-V characteristics has been achieved by two different methods. The first being annealing of the NW contact after contact fabrication. The second is by increasing doping concentration during NW growth. It is also shown that Pt/Ti/Pt/Au metallization is the layer configuration that exhibits the best ohmic contact and the most consistency in electrical measurements. 4-probe measurements were also carried out to measure the intrinsic resistivity of the NW, which makes it possible to estimate its doping concentration and carrier mobility.

NW/graphene contact was also tried.Mechanical exfoliation of kish graphite was performed to make high-quality graphene, which was selctively placed to make NW contact. However it is found that heating of the EBL-resist during e-beam evaporation caused the graphene to wrinkle and dissolve. CVD-grown graphene on Cu-foil was also tested. Inspection after the graphene transfer proved that the graphene that was used was incontinous and flaky making it difficult to obtain proper contacts to NWs. In addition the NWs connected to graphene probably suffered from over-etching due to multiple etching steps. Since a lot of efforts was put into obtaining a suitable measure of making NW/graphene contacts only preliminary measurements were conducted, so these results has yet to be verified.

Sammendrag

Kontakten mellom p-type GaAs nanotråder og elektroder har blitt undersøkt ved a fabrikere enkle nanotråd-enheter for så å måle elektroniske egenskaper. Både Au-assisterte og Ga-assisterte VLS-grodde nanotråder har blitt undersøkt, med størst vekt på Ga-assisterte nanotråder siden disse viste de beste elektroniske egenskapene for bruk i solceller. Nanotrådene ble grodd i et MBE-kammer, og de elektriske kontaktene ble fabrikert ved hjelp av elektronstrålelitografi og elektronstrålefordampning. Annealing ble brukt for å forbedre ohmsk kontakt. To typer kontakter ble undersøkt. Den første var metall/nanotråd kontakt hvor forskjellig metall strukturer ble brukt, inkludert metalliseringer som Pt/Ti/Pt/Au og Pd/Zn/Pd/Au. Den andre elektrode-typen var grafen som er forventet å vise veldig interresante elektriske og optoelektroniske egenskaper.

I denne oppgaven er det blitt vist at ohmsk kontakt og lineær I-V karakteristikk er blitt oppnådd ved hjelp av to forskjellige måter. Den første er å bruke annealing på kontakten etter den er fabrikert. Den andre er å øke dopingkonsentrasjonen under veksten av nanotråden. Det ble også konkludert med at Pt/Ti/Pt/Au var det beste metalliserings-oppsettet gav de mest ohmske kontaktene og også den beste kontinuiteten i elektriske målinger. Målinger med 4 prober ble også utført for å måle engenverdien til resistiviteten av nanotrådene. Dette gjorde det mulig å estimere dopingkonsentrasjonen og ladningsbærer-mobiliteten til nanotrådene.

Nanotråd/grafen kontakter har blitt testet. Dette viste seg imidlertid å være vanskelig å utføre. Overførselen av grafen til test-substratet viste at grafenen var ukontinuerlig og flakete, noe som gjorde at det var vanskelig å oppnå kontakt mellom nanotrådene og grafen. I tillegg forårsaket oppvarming under metalliseringen at grafenen ble rynkete, og nanotråder led antakelig av overetsing som følge av flere etsinger under denne prosessen. Mye innsats ble brukt til å klare å lage en måte å fabrikere målbare nanotråder/grafen kontakter. Det ble derfor kun utført innledende målinger av kontaktene, som viste seg å være ohmiske, men dette har til gode å bli verifisert.

Preface

This thesis was written as a part of the work that is performed by the nanowire group at NTNU regarding GaAs NW for optoelectronic devices device. The group is led by professor Helge Weman. Through the work I have performed for this thesis I have gained valuable knowledge. I have learned substantial amounts of physics regarding optoelectronics, semiconductors, band gap engineering and material science. I have also gained experience in working with nano and micromanipulation tools and microscopy in a clean room enviroment, and learned that research work is very detail oriented work, often with many unforseen problems, but in the end is very rewarding.

I would especially like to thank my supervisor, Dr. Dong Chul Kim, for devoting countless hours, sharing knowledge, providing training in the clean room and showing great passion for my work. He has also been of great motivation both through successfull experiments and frustrating tests. I would also like to thank professor Helge Weman for showing great interest for my results and suggesting interesting new experiments to be carried out, and the staff at NTNU nanolab for their helpfullness.

Lastly I would like to thank my fellow maste rstudents for their freindship and the motivation they have given me through these five years.

Ole Morten Christoffersen, Trondheim, 10.06.2012

Contents

1 Introduction **1**
- 1.1 Background . . . 1
- 1.2 Motivation . . . 1

2 Theory **3**
- 2.1 Gallium Arsenide . . . 3
- 2.2 Nanowires . . . 4
- 2.3 Doping . . . 4
- 2.4 Nanowire growth . . . 4
- 2.5 Ohmic contacts . . . 5
- 2.6 Graphene . . . 7
- 2.7 Graphene/NW contacts . . . 9
- 2.8 SEM . . . 9
- 2.9 Device fabrication . . . 10
  - 2.9.1 Electron Beam Litography . . . 10
  - 2.9.2 Surface Treatment . . . 10
  - 2.9.3 Metal Depostition . . . 11
  - 2.9.4 Annealing . . . 11
  - 2.9.5 Electrical Measurements . . . 12

3 Experimental **13**
- 3.1 Nanowires . . . 13
- 3.2 Single NW devices . . . 13
  - 3.2.1 Sample Preparation . . . 13
  - 3.2.2 Electron Beam Litography . . . 14
  - 3.2.3 Surface Treatment . . . 15
  - 3.2.4 Metallization and Lift-Off . . . 15
  - 3.2.5 2-probe measurements . . . 16
  - 3.2.6 4-probe measurements . . . 16
  - 3.2.7 Annealing . . . 17
- 3.3 SEM . . . 18
- 3.4 Graphene/NW contact fabrication . . . 18
  - 3.4.1 NW contacting . . . 18
  - 3.4.2 Graphene transfer . . . 19

3.4.3 Graphene contact . . . 21
3.4.4 Measurements . . . 23
3.4.5 Gate-dependence measurements . . . 23
3.5 List of samples measured . . . 24

4 Results and Discussion **26**
4.1 Overview of Previous Results on p-type GaAs NWs . . . 26
4.2 P-type NWs . . . 29
4.2.1 Processing . . . 29
4.2.2 Measurements; SC50 and SC96 . . . 31
4.2.3 Annealing; SC50 and SC96 . . . 32
4.2.4 4 probe measurements; SC96 . . . 36
4.2.5 Measurements; SC90 . . . 38
4.2.6 Annealing, SC90 . . . 38
4.2.7 4 probe measurements SC90 . . . 40
4.2.8 Measurements, As-589 7 . . . 42
4.2.9 Annealing, As589-7 . . . 44
4.3 Graphene NW contact . . . 45
4.3.1 Processing . . . 45
4.3.2 Measurements . . . 47
4.3.3 SEM of graphene contacts after measurment . . . 48
4.3.4 Gate-dependence measurements . . . 49

5 Conclusions and Future Work **52**

Bibliography **54**

Appendices **57**

A Other measured I-V characteristcs **57**

B Other images **66**

Chapter 1

Introduction

1.1 Background

The industrialization of nanotechnology is by many expected to mark a paradigm change within many fields of technology. Areas such as biotechnology, computer techology and materials science are areas where nanotechnology is currently under a lot of research. This thesis will investigate novel methods and structures in the field of photovoltaics with the aim to implement them in a solar cell device. Solar cells are by many thought to be an intriguing new large-scale energy harvester. The world is increasingly craving a reliable and large-scale renewable energy source. There is a vast potential in solar cells because the energy that radiates from the sun to the earth is many times more the energy need for the whole world and will continue to be so for the unforseeable furture. However solar cells are yet to be cost-efficient when compared to fossile fuels such as oil and coal. Other issues such as poor efficiency, poor energy absorbtion, lifetime and resistance to natural forces has yet to be resolved for industrial size use when the aim is to make it comparable to fossile fuels. The aim of this thesis will be to investigate methods of making energy absorption more efficient by fabricating and characterizing single nanowires (NWs) where the process steps themselves are tuned to make charge carrier transport through NW/electrode contacts as good as possible.

1.2 Motivation

The reason it is desirable to have high carrier transport through the contacts is that energy dissipation through resistive contacts and by carrier recombination is as small as possible to make energy transport as effecient as possible. To achieve this it is important to achieve ohmic contact to the NW. For GaAs this has proven to be difficult because GaAs tend to naturally form a schottky barrier at the GaAs/metal interface due to its high density of surface states. This barrier is difficult for charge

carriers to overcome in one bias direction, leading to a diode-like I-V characteristcs. This is especially prominent in NWs, as the NWs have a high surface to volume ratio, causing the surface state to have more effect on the contanct. The reason why these experiments with GaAs have been tested is because GaAs is a III-IV semiconductor that shows very promising optical properties. Recent studies has shown that p-type Ga-assisted GaAs NWs exhibit a more symmetric I-V characteristc compared to Au-assisted NWs. These Ga-assited NWs exhibits absence of diode-like characteristcs and high current in the order of 10s of μA. It is therefore interesting to see if real ohmic contact can be achieved[1].

Another interesting issue that will be discussed in this thesis is of the possibility to use graphene as electrodes for NWs. Graphene is a very promising material both in terms of electrical conductivity and optical properties. Since it is optically tranparent it is believed that charge carriers will uniformly be excited underneath the graphene in the NW. Since graphene also is a very good electrical conductor it may very well also function as an electrode.

Chapter 2

Theory

2.1 Gallium Arsenide

Gallium Arsendie (GaAs) is a III-V semiconductor(SC) which shows great promise in the area of opto-electronic devices. It is natural to compare GaAs to Silicon(Si) as Si is by far the most prominent SC in use for both CMOS and photovoltaic applications today. Unlike Silicon it has a direct bandgap (figure 2.1), which means that the lowest possible conduction band energy and the highest possible valence band energy is directly above each other. This makes electron excitation from valence band (VB) to the conduction band (CB) much easier. III-V semiconductors have the ability tune the band gap by altering their composition, which makes III-V SCs good absorbers for light ranging from near infra-red to ultraviolet wavelengths. GaAs has a larger absorbtion spectra then Si[2], and also has superior electron mobility. These properties makes GaAs a very promising material for fabrication of optoelectronic devices such as solar cells.

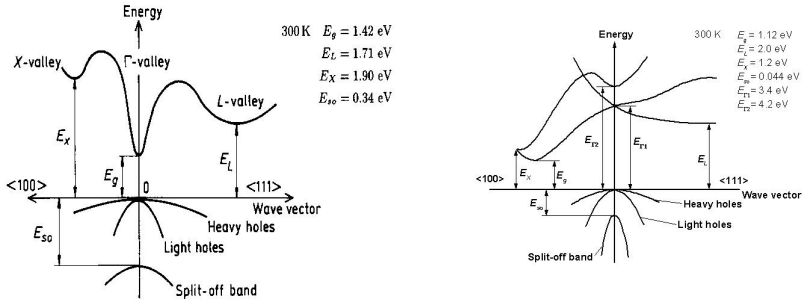

(a) (b)

Figure 2.1: a) GaAs band gap. b) Si band gap (from ref. 17).

2.2 Nanowires

Nanowires are wires that are constricted in 2 directions with a maximum diameter of about 100 nm. They are uncostricted in the 3rd plane, but are usually in the range of micrometers. The fact that it is constricted in 2 dimensions gives the NWs some interesting properties. Due to its high surface to volume ratio the density of surface states is much more prominent, and affects the NW in a larger extent than for bulk semiconductors. This leads to poorer electrical conductivity in a nanowire. However due to intrinsic anti-reflection property a dense array of NWs will yield very good absorbtion efficiency, making it ideal for solar cell devices[12, 13]. To transport the photo-generated energy as efficient as possible it is vital to have ohmic contact between the semiconducting NWs and the conducting metal.

2.3 Doping

Intrinsic NWs only consist of the elements described in the SC name (Si, GaAs, GaN etc). By introducing impurities to this compound it is possible to increase electrical conductivity. This process is called doping. 2 types of doping exist. N-type doping is introducing an element to the intrinsic semiconductor, which easily donates its electrons creating excess electrons in the semiconductor and thereby increasing the conducticity. These dopants are called donors and are typically group VI elemts like Te for n-type GaAs SCs. P-type semiconductors are made by introducing elements which easily binds to electrons in the semiconductor creating an excess of holes. These are called acceptors and are group II elemnets like Be for p-type GaAs SCs. The more impurities that are introduced the higher the doping concentration which is directly related to conductivity.

2.4 Nanowire growth

The vapor-liquid-solid(VLS) method in molecular beam epitaxy(MBE) is a method for NW growth. NWs are grown on a Silicon substrate with a thin native SiO_2 present on top due to air exposure. This oxide is etched using HF, creating Si pinholes in the oxide. Ga is then deposited on the substrate and forms liquid Ga droplets in the pinholes which act as a catalyst for NW growth[6]. Vapor Ga and As molecules are ejected from effusion cells and solidifies on the substrate. NW growth is caused by diffusion of the vapor through the catalyst droplet, causing the Ga and As to react and solidify beneath the catalyst[11]. Because Ga acts as the catalyst these NWs are classified as self-catalyzed NWs.

The doping process during growth in MBE is carried out by also ejecting the dopant element from a seperate effusion cell to create in-situ doping of the NWs. The dopant material is ideally diffused through the catalyst droplet, but can also diffuse through the NW sidewalls. When this happens the doping concentration

will be inconsistent throughout the volume of the NW, which may cause the NW to have uncontinous and location-dependant electrical properties[21, 22].

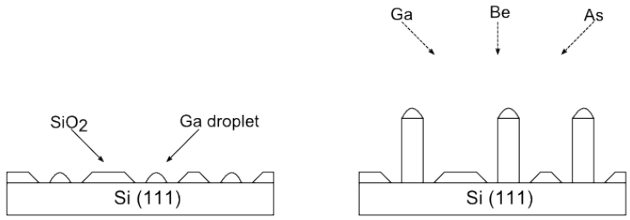

Figure 2.2: Nanowire growth schematic.

2.5 Ohmic contacts

The electrical I-V characteristics of an ideal ohmic contact is linear and symmetric which means that resistance through the contact is constant and that charge carriers can flow both ways with the same carrier density. This is desired for photon absorbers in solar cells. When a metal comes in contact with a semiconductor the Fermi level of the SC will align with the Fermi level of the metal causing band-bending of CB and VB of the semiconductor. In a p-type semiconductor the Fermi level lies close to the VB because the carge carriers are holes. As the electron affinity of the SC is smaller than the metal work-function the band interface between p-type SCs will be as shown in figure 2.3. Low-doped SCs tend to have a diode-like I-V characteristic where charge carriers only can flow in one direction and current increases suddenly after a certain voltage is applied. This is due to the formation of a Schottky barrier at the interface between metal and SC. This is a potential barrier caused by band-bending at the semiconductor which creates a recitifying junction where charge transport is greatly reduced in one bias direction. Ideal cases for Schottky and ohmic contact with respect to Schottky barrier hight are given in eq 2.1 - 2.2[2]

Ideal p-type ohmic contact

$$\Phi_m \geq E_g + \chi_{sc} \tag{2.1}$$

Ideal p-type schottky contact

$$\Phi_m - \chi_{sc} < E_g \tag{2.2}$$

However for NWs investigated in this thesis this is usually not the case, because the metal work function usually seems independent of the metal work function for GaAs[2]. This is believed to be due to Fermi level pinning. This occurs because GaAs has a lot of surface states on its surface. It is therefore expected that an

interface layer is formed between the metal and the SC. Charge carriers can overcome this barrier either by thermionic emmision or ballistic tunneling. If enough charge carriers tunnels through the Schottky contact the junction can be considered ohmic, but a requirement for this is that the barrier is thin and that the doping concentration of the semiconductor is high enough to generate a sufficient amount of charge carriers. For solar cell devices it is especially important to be able to create an ohmic contact to both p-type GaAs and n-type. This is because either a radial or longditudinal p-n junction NW is desired as a photon absorber in a solar cell device. The charge carrier mobility for a p-type GaAs structure (400 cm^2/Vs) is significantly lower than for an n-type GaAs structure (8500 cm^2/Vs). Recent STM measurements show for(001) GaAs that the Fermi-level pinning for p-type GaAs is dependant on doping concentration, whilst for n-type GaAs(001) it is independant on doping concentration(figure 2.4), which means that increasing doping should make the p-type contact more ohmic, at least for (001) GaAs[14]. Around a doping concentration of $10^{18}cm^{-3}$ for p-doped GaAs the Fermi level would be realxed and drop toward the VB level.

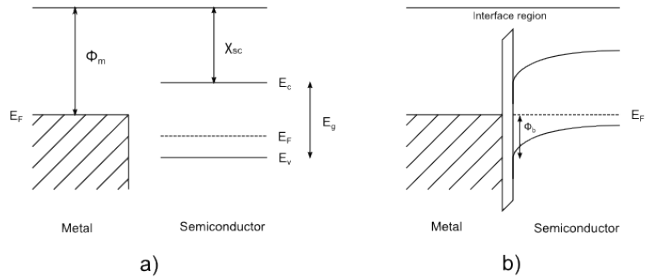

Figure 2.3: Interface between metal and p-type semiconductor.

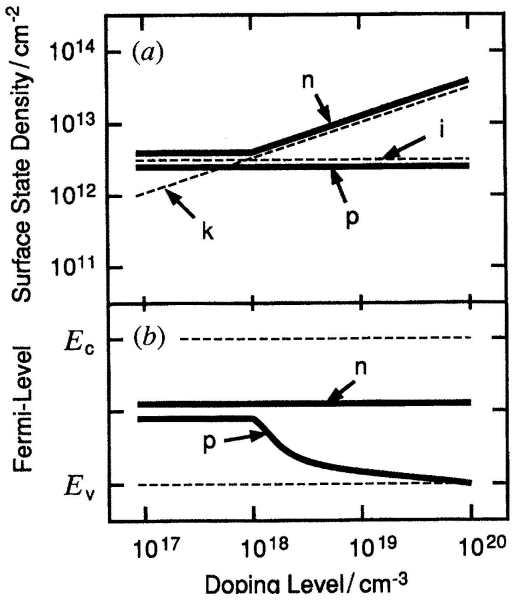

Figure 2.4: Fermi level pinning for both n-type and p-type GaAs relative to doping concentration (from ref 14).

2.6 Graphene

Graphene is a single atom layer of carbon atoms arranged in a hexagonal honeycomb structure[15]. It has zero band-gap on 6 points in the 1st Brillouin zone, which are known as Dirac points (figure 2.5), which makes it a zero band gap semiconductor. Graphene has superior mobility with a theoretical value of $200000 cm^2/Vs$ with low corresponding resistivity of $10^{-6}\Omega cm$. However it should be mentioned that when the graphene is dispersed on SiO_2 which is the case in this thesis scattering of electrons by optical phonons on the substrate limits the electron mobility to $40000 cm^2/Vs$, and that experiments has yet to show a value of above $15000 cm^2/Vs$. This is still a very high mobility, which makes it a very interesting material for novel opto-electronic devices. The electrical conductivity of the graphene is limited by its 2d structure, so resistivity is always higher than the theoretical value. Experiments have shown that charge transport should be almost equal for holes and electrons. Monolayer graphene is optically transparent as can be seen from figure 2.6. While the transmittance decreases while layers are increased the graphene still show very good transmittance for several layers (89 percent for 5 layers).

In addition to being optically transparent an interesting property of graphene is the tunability of its work-function. This is done by applying an external gate voltage to the graphene[15]. This way it is possible to tune the fermi level near

the CB/VB interface and thus deciding wether the graphene is to exhibit n-type or p-type behaviour. According to Geim and Novoselov this change happens around a gate voltage of 40 V (figure 2.5 b)).

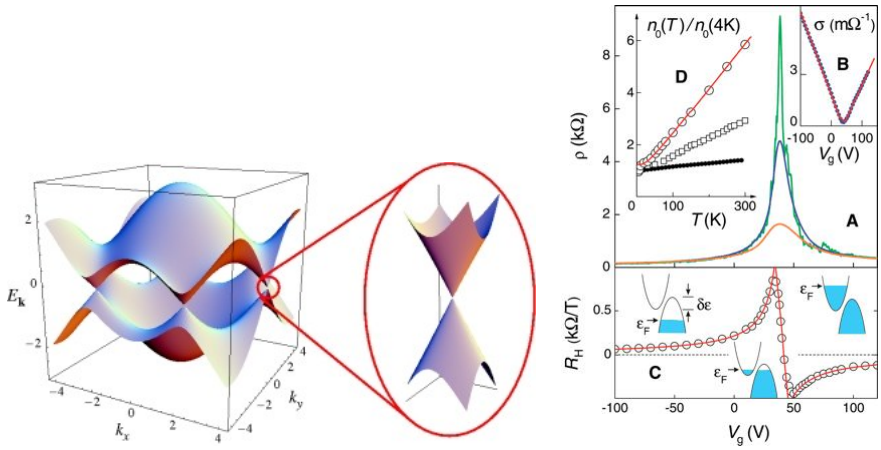

(a) (b)

Figure 2.5: a) Band structure of graphene. b) Gate voltage dependence of carriers and resistivity in graphene (from ref 15).

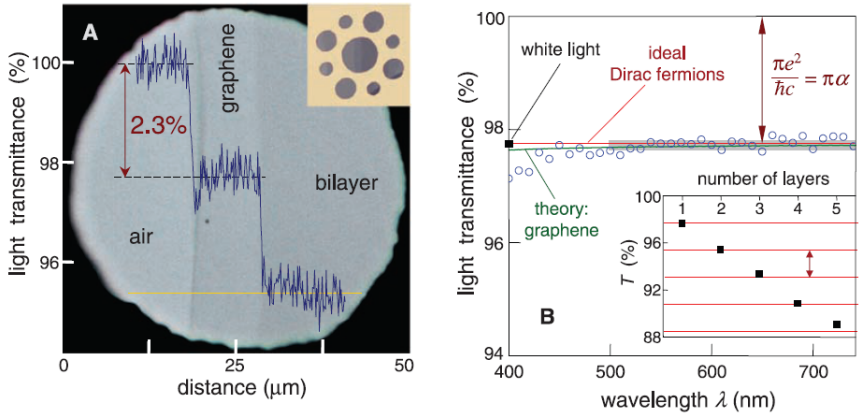

(a) (b)

Figure 2.6: Graphene transmittance in relation to a) distance, b) wavelength. (From ref 26)

2.7 Graphene/NW contacts

Contacts between NWs and graphene is an intriguing and novel method of carrier transport in photovoltaic devices. Because of graphenes low resistivity it can function well as an electrode. However the most exciting aspect of it is that it is optically transparent. In theory light should therefore be absorbed through the lenght of the NW and not just through the parts that are not covered by metal. This should cause the excitation of charge carriers throughout the lenght of the NW making it uniform in charge generation, instead of just creating charges at a certain position on the NW.

Since it is possible to tune the carrier type of the graphene near the dirac points it is possible to tune the carrier concentration and carrier type that are injected in the NW from the graphene. It is then possible to carry out electronic and optical measurements while tuning carrier concentration and altering carrier type, making very interesting p-n junction measurements possible.

2.8 SEM

The scanning electron microscope is an important tool for characterization of nanostructures because of its ability to create high resolution images. It is also an integral part of the electron beam litography system in NTNU nanolab which will be discussed later. In the SEM electrons are accelerated with typical voltages of 5 - 20 kV. The electrons are then emmited by the electron gun and hits the sample with great speed. Back-scattered electrons(BSE) and secondary electrons(SE) are then registered at a sensor and analyzed. These electrons give information about the topography of the surface and can therefore create an image of the surface of the sample. SE are electrons that are scattered immidiately from the surface and BSE are electrons that penetetrate the sample and resurfaces.

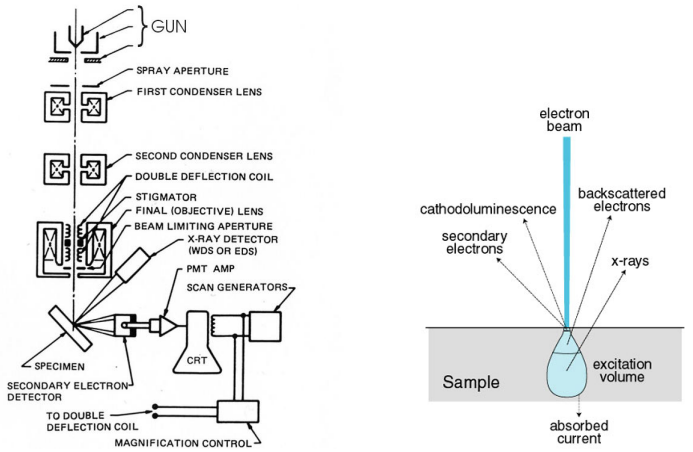

(a) (b)

Figure 2.7: a) Schematic of SEM. b) E-beam/sample interaction schematic. (from ref 20, 21)

2.9 Device fabrication

2.9.1 Electron Beam Litography

Electron Beam Litography(EBL) is a method of creating nanosized structures on a substrate. The advantage of EBL is that it does not need any sort of prefabricated pattern to transfer a designed pattern to the substrate as is the case for instance for photolitography or nano imprint litography. Another advantage is its ability to make highly precise nanostructures with a feature resolution below 100 nm.

The EBL setup used for this thesis consists of a SEM and an electron beam movement control. Using the movement control it is possible to swipe the electron beam very precisely over the areas of the sample which is to be exposed. When the electron beam from the SEM hits the EBL resist long polymer chains in the resist break up and are easily soluble. Because of the mask-less exposure this method is very advantegeous in experimental designs such as in this thesis because electrode design is different from sample to sample due to different NW position. However due to very low throughput it is very unsuitable for industrial large scale fabrication.

2.9.2 Surface Treatment

Surface treatment is a process which is supposed to remove all exterior effects on the NWs. Though the fabrication of these devices is done in a clean room enviroment there is still some contamination and chemical effects on the substrate, which is undesirable. To remove contaminants and carbonic residues the NWs are subjected

to oxygen plasma ashing. An RF source is ignited in a vacuum chamber which holds an O_2 enviroment. This accelerates O_2 ions between the cathode (chamber walls) and anode (sample). Since these ions are electrically charged they react with the contaminants on the sample and creates an oxygen ash which is easily removed.

Thin oxide layers spontaneously form on the substrate and on the NWs when the sample comes in contact with air. This is undesirable as the contact between the GaAs and the metal should be as clean as possible. This is easily removed by etching the sample using HCl. This process also removes the oxygen ash that was made in the oxygen plasma ashing.

2.9.3 Metal Depostition

Electron beam evaporation is a method of depositing metal on a substrate which uses an electron beam to heat a metal target. The metal then evaporates and hits the sample causing a thin film layer to be formed. The electron beam is created by a tungsten filament and electrons are accelerated with a voltage of several kVs. The evaporated metals then elevate in the chamber. The sample is placed upside-down over the metal crucible. High-vacuum in the chamber yield a long mean free path for the particles so that a close to uniform layer solidify on the sample. This is a highly controllable metal deposition method and can yield such a low deposition rate as 0.1 Å/s. This gives a very good control of layer thickness. The deposition rate is measured by a piezoelectric crystal which measures the mechanical stressed caused by added weight of the metal that adheres to it, and sends an electric signal which is interpreted as deposition rate.

2.9.4 Annealing

Annealing is a heat treatment with the intention of increasing ohmic contact between semiconductor and metal. This is desired in such semiconductors as GaAs which has a large amount of surface states that disrupt ohmic contact. Diffusion due to heat causes interface layers in the metal configurations where both layers are represented. When a contact is annealed the particles from the metals penetrate into the layer below, and if layers are thin enough they penetrate even further[6]. This effect increases with temperature. This way particles from the metals which acts as dopants for GaAs can penetrate into the NW itself and create a highly doped layer near the surface of the NW (figure 2.8 a). Then more carriers can flow between the metal and the semiconductor, enhancing ohmic contact. The other way of enhancing ohmic contact through annealing is that the amoprhous interface layer between SC and metal allows mutual transmission of charge carriers (figure 2.8 b)[10]. However too high temperature may damage the NW itself or the contact structure.

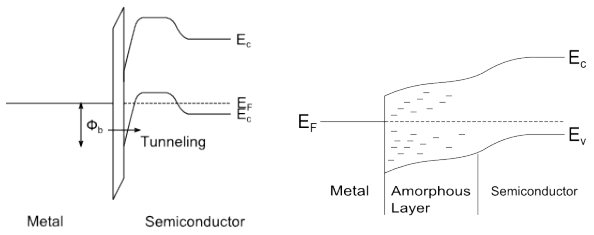

Figure 2.8: a) Heavy doping of p-type SC/metal contact. b) Amorphous layer at SC/metal interface.

2.9.5 Electrical Measurements

Electrical measurements of such small features are usually done in a probe station where probes connected to the desired electrodes completes a circuit with a signal generator. The probes are very fine metallic tips which can accurately be placed with an electrode smaller than 100x100 μm with the aid of an optical microscope. 2-probe measurements are usually done to check the current through the NWs and the electrode contacts. With a 4-probe meausrement configuration it is possible to measure the reisitivity of the NW itself. In usual 2-probe measurements a contact resistance is always added when a semiconduting NW comes in contact with a conducting metal. In addition voltage offsets can be created by space charges at the Schottky barrier. However, by measuring on 4 probes one can bias the current through 2 probes and measure the voltage drop over the NW by 2 seperate probes. This way the real resistance of the NW can be calculated. No current is flowing over the 2 seperate probes that measures voltage drop and therefore contact resistance is prevented. By averaging voltage caused by negative and positve current the bias voltage offsets are prevented.

When the real resistance of the NW is known it is possible to the resistivity and therefore calculate a good approximation for carrier concentration and carrier mobility for the NW. By using equation 2.3 and 2.4. L = mid-electrode distance, r = NW radius and mu_h = hole mobility.

Resisitivity

$$\rho = \frac{R(\pi r^2)}{L} \tag{2.3}$$

Carrier concentration

$$n_h = \frac{1}{\rho e \mu_h} \tag{2.4}$$

Chapter 3

Experimental

3.1 Nanowires

Several different types of NWs were tested for this thesis. P-typed Ga-assisted with different doping concentration (SC50, SC96, SC90), where SC50 and SC96 are grown with a Be source temperature of 990°C which will give a doping concentration of approximately $3*10^{18}cm^{-3}$ for thin film. SC90 is grown with a Be source temperature of 1025°C which will yield a doping concentration of $1*10^{19}cm^{-3}$ for thin film. P-typed Au-assisted (As589-6, As589-7) are also grown with a Be source temperature of 990°C, same as SC90 and SC 96. All NWs were grown by the VLS-method in MBE.

3.2 Single NW devices

3.2.1 Sample Preparation

After growth NWs are dispersed on the $SiO_2(300nm)/Si$ substrate for device fabrication. The substrate is 5x5 mm and covered with gold pads making up a grid of 16 positions each with a possiblity of 12 contacts.

NWs were dispersed on the substrates mainly by a wet transfer method. This method is carried out by dipping the substrate with the as-grown NWs in a solution of Isopropanol. The solution is then sonicated in water for 30 seconds, before a droplet of the solution is dispersed on the test substrate. The substrate is subsequently air-dryed to make sure all NWs are deposited on the surface. In a few cases NWs were also transfered using a dry transfer method. This is a basic method by dragging a paper over the as-grown NWs and then dragging the same paper over the test substrate. Some NWs then stick to the surface.

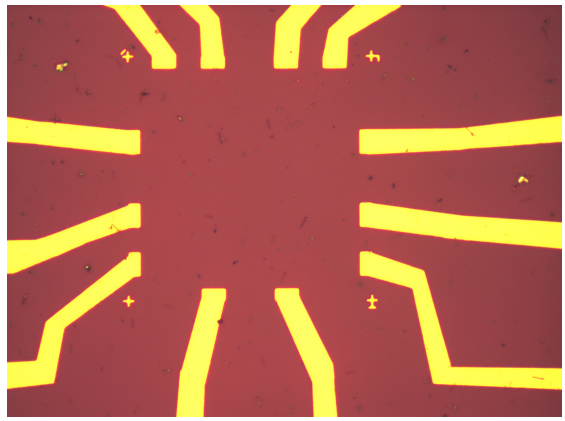

Figure 3.1: Substrate after dispertion.

3.2.2 Electron Beam Litography

The NW contacts were designed using Clewin, a design software for micro and nanosized litographic methods. Both 2-probe and 4-probe contacts were designed. For the EBL positive resists were used as this is most reasonable when it comes to metallization. The EBL resist was then spun on using a spin coater at 4000 rpm for 2 minutes with an acceleration speed of 1000rpm/s^2. For the NW contacts a double layer of resist was used, so thick metallization could be obtainable whilst increasing the effect of undercutting. PMMA 200K and PMMA 6.5 were used resulting in a resist thickness of about 1 um. The EBL alignment and exposure was then carried out.

After EBL exposure the pattern was developed. This was done in a solution of Isopropanol and DI water (9:1). Development time varied a little bit each time, but 30 seconds was usually sufficient. This was therefore set as a default development time. An inspection in an optical microscope would tell if the pattern was fully developed or not.

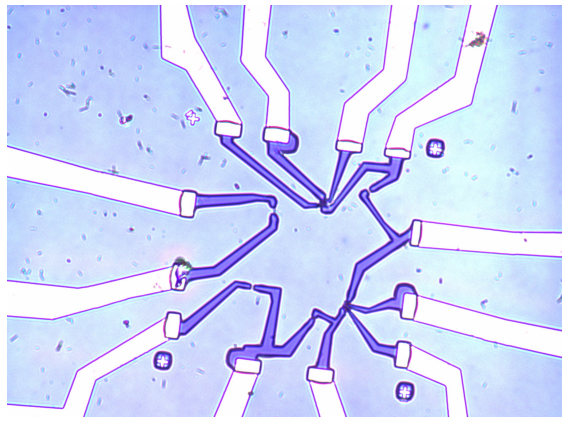

Figure 3.2: Substrate after development.

3.2.3 Surface Treatment

Surface treatment was done using oxygen plasma ashing and wet etching before metallization. Plasma ashnig was done in a plasma cleaner with O_2 at 50 W and 0.35 mbar for 12 s. Wet etching was done in a solution of 37 percent HCl and DI water (1:10) for 10 s. After etching the sample was rinsed thoroughly with DI water. It is important that the time interval between these two steps and between etching and loading in the evaporator is as fast as possible in order to minimize the risk of contaminating the sample and preventing an oxide layer from forming on the NWs.

3.2.4 Metallization and Lift-Off

Metallization was carried out in the e-beam evaporator with an acceleration voltage of 8 kV. Different currents were used for different metals as the different metals have different melting temperatures. Over time the beamspot position and current needed to heat the metal are changed. This means that the e-beam regularly has to be calibrated. However table 3.1 shows typical metallization parameters used. It is important that the deposition rate is low enough to make a uniform layer, but high enough that the substrate is not overheated. Some samples were metallized in IBM Zurich.

Metal	Current	Deposition rate
Au	50 mA	10 Å/s
Pt	135 mA	1-3 Å/s
Ti	40 mA	2-3 Å/s

Table 3.1: Table of typical currents for metallization in the e-beam evaporator.

Lift off was performed by bathing the metallized sample in acetone overnight. This was usually not enough to move undesired regions of metal and EBL-resist, but dissolved the resist to such a degree that it could be easily removed by spraying the sample with acetone.

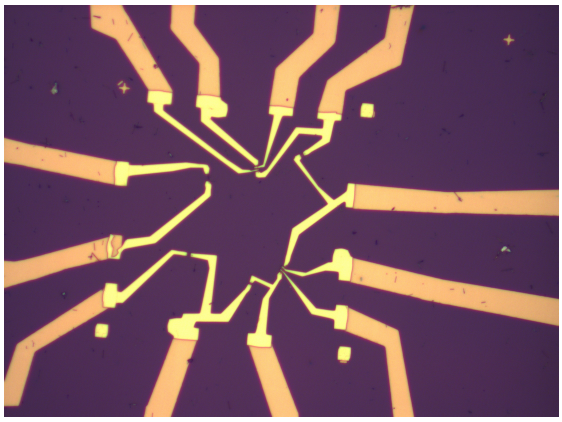

Figure 3.3: Substrate after lift-off.

3.2.5 2-probe measurements

2-probe measurements were carried out by connecting 2 probes to the specified gold pads that represented each end of the NWs. These were connetcted to a Keithley 4200-SCS (Semiconductor Characterization System), creating a full circuit. A 3 V sweep with 100 mV intervals was applied over the electrodes and the current and resistance of the individual NWs were measured. Open and short circuit current was measured before the actual NWs to check if the system was working properly.

3.2.6 4-probe measurements

The 4-probe setup consist of 2 outer probes, and 2 inner probes, completing 2 seperate circuits. A square AC pulse with 3 periods is applied over the outer probes . Several current are applied (50nA, 100nA, 500nA, 1uA and 5uA) to get good statistics. The voltage drop over the two inner probes(A and B, figure 3.4) is then measured. Resistance is calculated using Ohms law. The voltage occuring due to negative current is subtracted from the voltage occuring due to postive current, and they are then averaged. This is done to remove any spurios signals from heating effects or space charges at the Schottky Barriers. The voltages are then averaged and divided by current to calculate resistance (eq. 3.1 - 3.3).

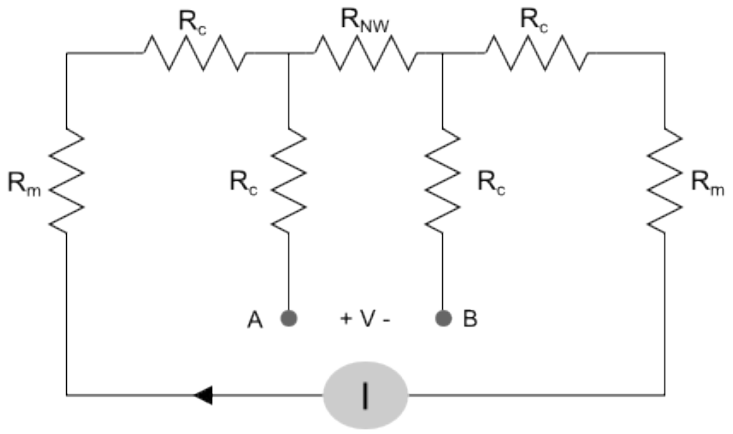

Figure 3.4: 4-probe measurement setup

$$\frac{V^+ - V^-}{2I} = R_{NW} \tag{3.1}$$

$$V^+ = I^+ * R + I * R^2 + V_{offset} \tag{3.2}$$

$$V^- = I^- * R + I * R^2 + V_{offset} \tag{3.3}$$

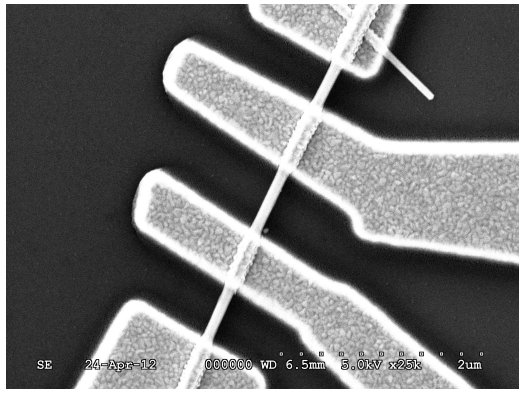

Figure 3.5: SEM image of a NW with 4-probe contact.

3.2.7 Annealing

Annealing was performed in a rapid thermal processing unit(RTP). The sample was placed on a Si wafter that is connected to a thermocouple. Initial temperature

in the chamber is 20°C. The chamber is then pumped down to a feasable vaccum level before it is purged with nitrogen. The lamp elements were then heated to the desired temperature in 10 seconds. The sample is then heated at that temperature for 30 seconds before the heating lamps are turned off. This is followed by a 3 minute relaxation step where temperature is decreased by water cooling and the chamber is then ventilated.

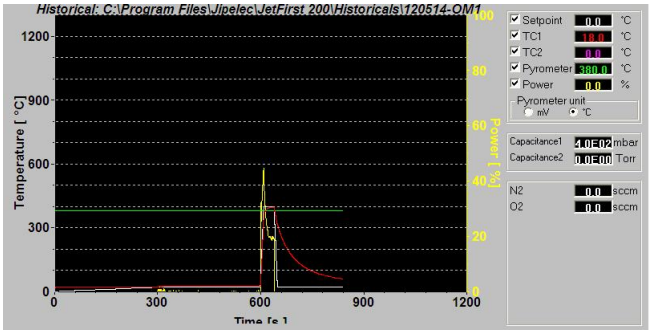

Figure 3.6: Graph showing temperatur and other parameters during an annealing.

3.3 SEM

High resolution images of the NW contacts were shot by scanning electron microscopy (SEM) which is the basis for the EBL set up. Instead of using 20kV acceleration voltage 5kV was used to minimize damage on the sample. This also means that a lot of electrons are scattered mainly at the surface, which means the surface topography becomes clearer, but the depth of focus decreases. However the NWs and contacts are thin enough to not be affected by this. Images were taken to identify if there were any damages or abnormalities that happened during annealing.

3.4 Graphene/NW contact fabrication

3.4.1 NW contacting

NWs were contacted in exactly the same way as for single NW devices with the exception that only one side of the NW were contacted. This is to make place for the graphene to act as electrode on the other side.

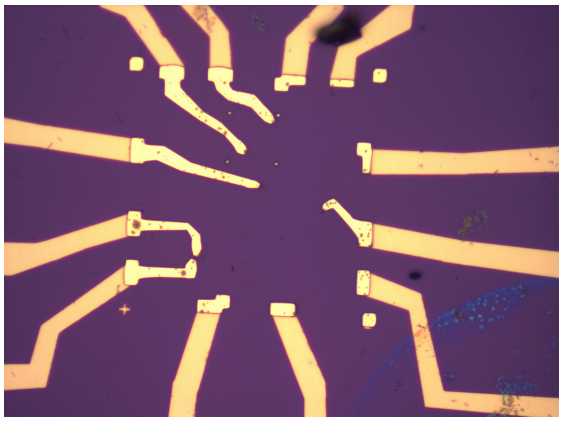

Figure 3.7: SC90-3 after metallization with only 1 electrode.

3.4.2 Graphene transfer

2 different types of graphene transfer to the substrate were used. In the first method performed at NTNU graphene was extracted from Cu foil covered with graphene on both sides. The Cu foil was straightened to be as flat as possible. After straightening, the graphene on one side was removed using oxygen plasma at 0.50 mbar and 90 W power for 5 minutes. The single side which holds graphene was then spin coated with PMMA A2 at 4000 rpm for 2 minutes with an acceleration speed of 1000 rpm/s^2 before it was soft-baked at 160 °C for 2 minutes. This step is necessary because once the Cu foil is removed this will act as a scaffold to keep the graphene from breaking up into smaller pieces during cleansing. The Cu foil was then removed by bathing the sample in an iron nitrate solution overnight. The iron nitrate was diluted in DI water in the relation $Fe_2N_3O_9 \bullet 9H_2O$: DI 0.5:100. This treatment etches all of the Cu foil, so only the PMMA with the graphene underneath is left. The graphene is further cleansed using a solution of HCl : H_2O_2 : DI 1:1:20 for 15 minutes and NH_3 : H_2O_2 : DI 1:1:20 for 15 minutes[24]. This was quite a time consuming process because the process has to be done in the same container that holds the graphene and iron nitrate solution to prevent the graphene from wrinkling. All solutions were therefore added and extracted using 10 ml vaccum beaker. In between each solution the previous solution was diluted with DI water. To make sure the solution was properly diluted this had to be carried out at least 3 times for every solution. The substrate was then surface treated in the same manner as for single NW devices before the grahene and PMMA was transfered to the substrate by simply scooping it onto the substrate. The PMMA was then removed by bathing the sample in acetone, so eventually the substrate was covered with a layer of graphene.

The second method was performed in Korea by professor Sang-Wook Lee's group at Konkuk University (Physics department). This method has many similarities with the process carried out at NTNU, including using PMMA as a scaffold to

transfer the graphene between substrates. However this method used mechanically exfoliated graphene, which is a method of dividing a piece of single crystalline kish graphite enough times to ultimately have just a few-layer or single layer sheet of graphene left. This method used SiO_2 as the initial substrate in stead of Cu. The SiO_2 was also etched away after PMMA spin coating so only graphene and PMMA were left and then transported to the target substrate. However the main difference in this method was the ability to accuratly manipulate and selectively place the graphene with PMMA on the substrate using micro-manipulation tools. This made sure that the graphene sheets were accurately placed on the desired positions on the substrate. However since mechanically exfoliated graphene usually yield smaller sheets, with a size less than 100 x 100 μm^2, there was a need to further contact the graphene by creating more metal electrodes, so a complete circuit could be realized.

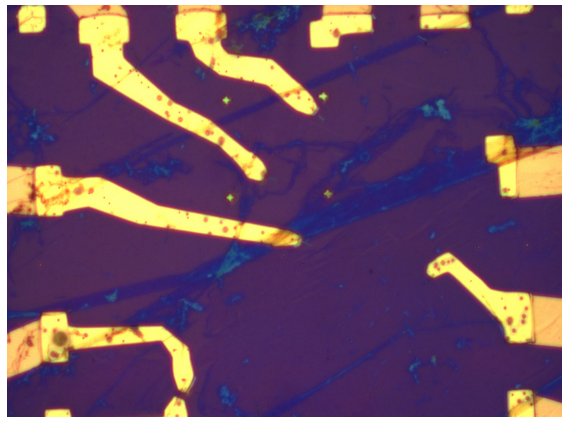

(a)

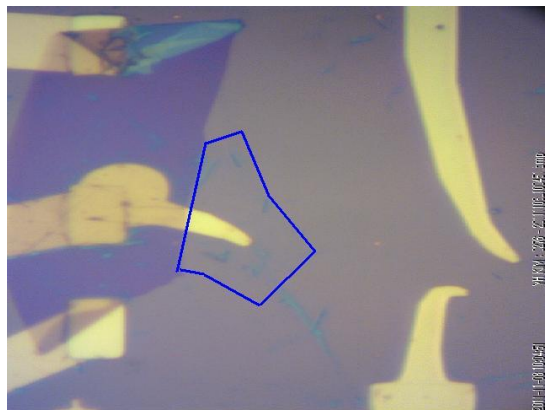

(b)

Figure 3.8: a) SC90-3 after graphene transfer performed in NTNU. b) SC50-7 after graphene transfer performed in Korea.

3.4.3 Graphene contact

The graphene was then trimmed to make sure it did not shorten any electrodes. For the samples processed in NTNU this was done by applying a negative resist on top of the substrate and design a pattern so that the graphene was trimmed in such a manner that some electrodes were contacted to the graphene and some to the NWs, while the NWs and GP are in contact (fig. 3.9 b). The resist that was used was negative ER ma-N 2401 which was spun on at 3000 rpm for 60 seconds with an acceleration speed of 500 rpm/s^2. The sample was then soft baked at 90°C for 3 minutes. EBL was performed in exactly the same way as for single NW devices. The sample was then developed using the developer ma-D 525 for 30 seconds. The resist remover that was used was mr-REM 660 overnight.

In the method performed in Korea new metal contacts were fabricated that were exclusively connected to the graphene. The metal contacts were fabricated using Cr(5 nm) and Au(100 nm). These contacts were also fabricated in the e-beam evaporator. This had to be done because that graphene did not cover any of the pre-fabricated electrodes, as was the case with the graphene transfer performed at NTNU (fig 3.9 a). This is because the selective placed graphene sheets are much smaller than the sheets transfered in NTNU.

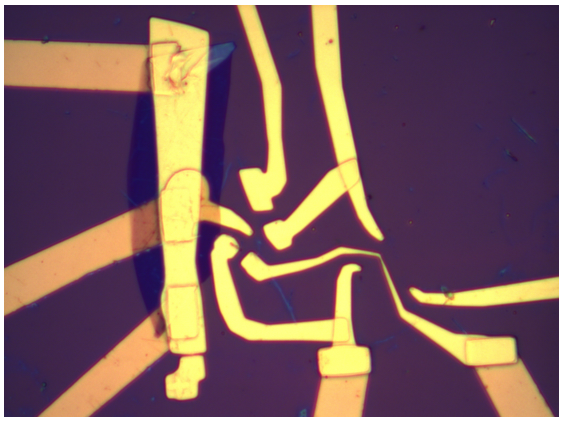

(a)

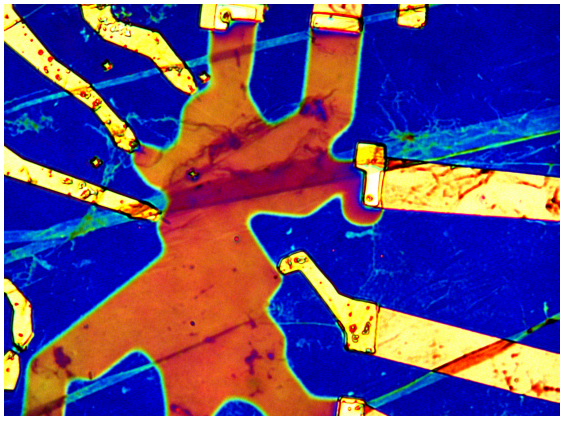

(b)

Figure 3.9: a) SC50-7 after fabriacting metal contacts to graphene. b) SC90-3 after development of negative resist EBL.

After the resist had been developed to create a pattern that made sure NW and the graphene were connected to seperate electrodes the final step was to etch the excess graphene so that graphene did not shorten the electrode that was connected to the NW. This was done using oxygen plasma ashing. The parameters for this was 0.30 mbar flow and 50 W power. The time that had to be applied was different for the methods. 1 minute was sufficient for the selectively placed graphene while 2 minutes had to be applied for the graphene transfer performed in NTNU due to the PMMA residue that was left on the graphene after the transfer. This residue can be clearly seen in figure 3.9 b).

(a)

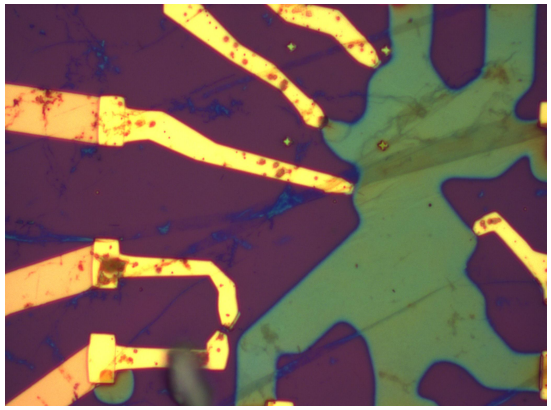

(b)

Figure 3.10: a) SC50-7 after graphene trimming. b) SC90-3 after graphene trimming.

3.4.4 Measurements

The measurements were done excactly the same way as for 2-probe masurements where one of the gold pads is cconnected to the NW and one was connected to the graphene.

3.4.5 Gate-dependence measurements

Gate dependence measurements were conducted to confirm that the graphene on the sample coincided with earlier results concerning gate voltage measurements[15]. Two types of measurements were conducted. One with bare graphene connected

to both source and drain, and one where graphene was connected to one end of a NW. Gate was connected to the back-gate i.e. the back side of the substrate. Two samples were measured. SC90-3, which contained NW and graphene was subjected to a gate voltage sweep of -30 to 30 V. The reason this voltage was applied is that it is believed that higher voltages might damage the back-gate causing leakage current and thereby comprimising the entire sample. This was carried out to confirm that the trend for Ig was as expected from earlier experiments performed by Geim and Novoselov, both for NW/graphene and excluively graphene. The other sample measured (SC90-5) was solely graphene contacts and was therefore subjected to higher voltages, up to 60 V, to check if the graphene exhibited the well-known current change at the Dirac point which relates to the altering of the graphene Fermi level. This is expected to happen around 40 V.

3.5 List of samples measured

Sample	Contact	Growth Catalyst	Doping	Annealing	Comments
SC50-5	M/NW/M	Ga	α	400° C	
SC50-15	M/NW/M	Ga	α	360° C	
SC96-1	M/NW/M	Ga	α	400° C	
SC90-1	M/NW/M	Ga	β	400° C	
SC90-2	M/NW/M	Ga	β	380° C	
SC90-6	M/NW/M	Ga	α	400° C	
As589-7-1	M/NW/M	Au	α	400° C	
As589-7-2	M/NW/M	Au	α	380° C	

Table 3.2: Sample processing, single NW devices. α correspond to an expected soping level of $3 * 10^{18} cm^{-3}$, while β corresponds to an expected doping level of $1 * 10^{19} cm^{-3}$.

Sample	Contact	Growth Catalyst	Doping	Comments
SC50-7	M/NW/GP/M	Ga	α	graphene gone after processing
SC50-8	M/NW/GP/M	Ga	α	graphene gone after processing
SC96-2	M/NW/GP/M	Ga	α	No contact
SC90-3	M/NW/GP/M	Ga	β	
SC90-5	M/NW/GP/M	Ga	β	No contact

Table 3.3: Sample processing. NW/graphene devices

Instrument	Type
Optical Microscope	Zeiss Scope A:1 Ax10
SEM	Hitachi S-4300SE
EBL	Raith Elphy Plus
E-beam Evaporator	Pfeiffer Vacuum Classic 500
Plasma Cleaner	Diener Electronics Femto
RTP	Jipelec Jetfirst

Table 3.4: Table of instruments used

Chapter 4

Results and Discussion

4.1 Overview of Previous Results on p-type GaAs NWs

Earlier results acheived by the NW group at NTNU has shown that ohmic contact to p-type GaAs NWs are difficult to fabricate. For Au-assisted NWs the results are very inconsistent and a lot of the NWs meausered show diode-like behaviour. However for Ga-assisted almost all NWs show symmetric behaviour though not completely ohmic and linear[1]. This is believed to be due to the fact that the Au catalyst probably stays solid throughout the growth process. When Gold reacts with Berylium the melting temperature increases significantly[11]. This makes it hard for the vapor Ga, As and Be to diffuse through the catalyst droplet, and instead diffuse through the side walls, causing shorter NWs and lower doping concentration.

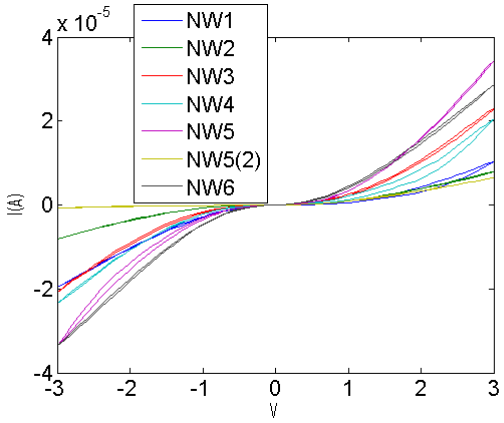

Figure 4.1: I-V characteristics of SC50-2, Self-catalyzed Be-doped NWs.

The focus has therefore recently been devoted to Ga-assisted core Be-doped GaAs NWs. Several process parameters has been altered to try to make ohmic contact between conducting metals and NWs. Surface treatment steps included HCl etching and surface passivation with ammonium nitrate. It was established that surface passivation, which prevent the formation of an oxide layer, had very little effect if any at all. HCl etching is important to remove the oxide layer on the NW surface before metallization. This was first applied as a very diluted solution and later tried with a "stronger" solution, but this increase also had little effect, which indicates that the diluted solution is sufficient to etch away the oxide entirely.

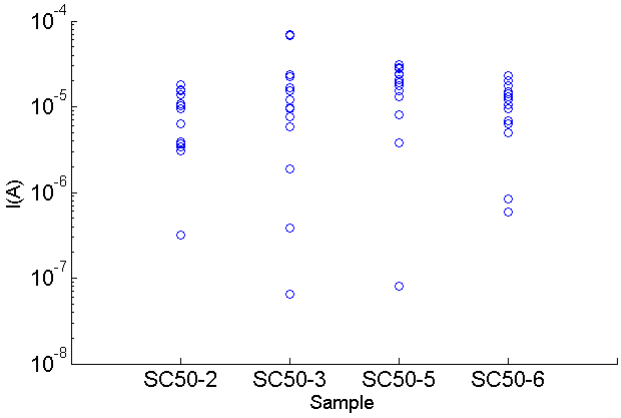

Figure 4.2: I measured at 3 V for NWs with different surface treatment parameters. SC50-2: Weak etching, no passivation, SC50-3: Weak etching, weak passivation, SC50-5: Strong etching, weak passivation, SC50-6: Strong etching, strong passivation. See table 4.1 for parameters.

Weak etching	$HCl : H_2O$ (1:10) for 10 seconds
Strong etching	$HCl : H_2O$ (1:1) for 10 seconds
Weak passivation	$NH_4S_x : H_2O$ (0.02:10) for 2 min
Strong passivation	$NH_4S_x : H_2O$ (1:9) for 2 min

Table 4.1: Table of surface treatment parameters.

Several different metallization configurations were also tested, including Pt/Ti/Pt/Au, Pd/Ti/Au, Ti/Au, and Pd/Zn/Pd/Au. It was concluded that Pt/Ti/Pt/Au gave the best I-V characteristics, and focus was therefore given to this metallization setup. As can be seen from figure 4.3. Pd/Zn/Pd/Au also gives good I-V characteristics, however after metallization this looked not as good when inspecting the sample in an optical microscope.

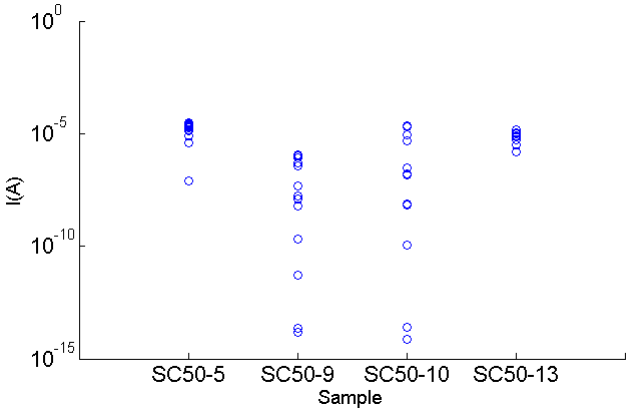

Figure 4.3: I at 3 V for NWs with different metallization schemes. SC50-5: Pt/Ti/Pt/Au. SC50-9: Pd/Ti/Au. SC50-10: Ti/Au. SC50-13: Pd/Zn/Pd/Au. See table 4.2 for metal thickness.

Pt / Ti / Pt / Au	5 nm / 10 nm / 10 nm/ 150 nm
Pd / Ti / Au	40 nm / 10 nm / 70 nm
Ti / Au	10 nm / 120 nm
Pd / Zn / Pd / Au	10 nm / 3 nm / 40 nm / 207 nm

Table 4.2: Table of metal thicknesses.

Annealing was tested to check if this would enhance current and ohmic charateristcs. 300, 320 and 350 °C were tested, and though it showed a slight improvement, it was not enough to make a significant impact. It was also believed that the NWs were significantly damaged at 350°C, however this was tested on already annealed samples.

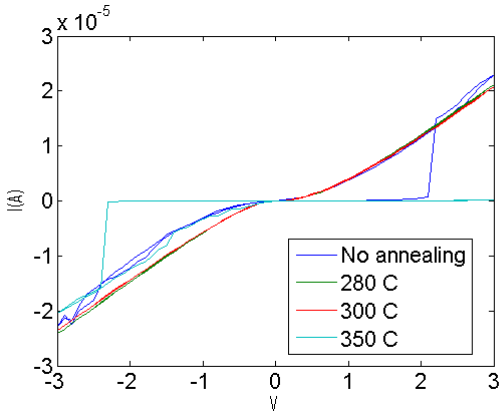

Figure 4.4: I-V characteristics after several annealings

Lastly 4-probe-measurements were conducted on 2 NWs to determine the contact resistance and the real resistance of the NWs. NW 1 showed a 2-probe resitance of 87 $k\Omega$ and a 4-probe resistance of 60 $k\Omega$ which makes the contact resistance 27 $k\Omega$. This contact resistance is 32 % of the entire resitance. For NW 2 the 2-probe measurement was 107 $k\Omega$ while 4-probe resistance was 83 $k\Omega$. This makes for a contact resistance of 22 % which is fairly consistent due to fluctuations. The resistivity that was calculated for these NWs were $308 \bullet 10^{-4} \Omega cm$ and $597 \bullet 10^{-4} \Omega cm$

4.2 P-type NWs

4.2.1 Processing

Processing parameters for contact fabrication to p-type GaAs NWs have already been discussed in the previous report[1] so the parameters from that report has been used succesfully used in this thesis, however there were some issues regarding the fabrication of single NW devices that should be discussed. Though the dry transfer of NWs from growth substrate to test substrate is an easy way of transferring NWs in this project wet transfer was preferred. This is because for some of the samples it proved to be difficult to dispatch the NWs on the test substrate via dry-transfer. They broke off from the test substrate easily enough but was difficult to get off from the paper. In addition wet transfer gives a more uniform distribution of NWs on the substrate. Dry transfer tend to form clusters of NWs at certain positions.

Another issue that was prominent was heating in the e-beam evaporator. This caused the EBL resist to start bubbling and thereby caused the metallization to become very uneven, which again affected the alignment and morphology of the metal electrodes. Though most of the electrodes still contacted the NWs it is difficult to determine defects in the contacts when taking SEM pictures because the metallization already looks bad. This is especially important after annealing when

it is important to determine whether high temperatures has caused any damages to the contact or the NW itself. Excactly why this bubbling occured is difficult to determine, especially when it has worked fine in previous experiments. However when changing materials in the evaporator several metallization parameters often have to be altered to make the metal heat enough to vaporize. This is because of volume in the metal crucible and metal quality. This often causes amplitude, position and most important current magnitude of the electron beam to change. In the experiments where bubbling occured many of these currents were higher than they used to be before, which causes the chamber to have a higher temperature. This is one theory of why the resist started to form bubbles. To try to prevent this it was tried to increase the current even more to get faster deposition rates and thereby minimize the time the substrate was exposed to the source in an attempt to reduce possible heating during evaporation. This proved to have little effect. To find out which material was causing the problems each metallization was tried on different test substrates. When this was tried all the samples had a perfecly even surface. It was therefore suggested to ventilate the sample between each metallization layer. This however could not be carried out without the risk of compromising the sample. Since the Pt layers are very thin it is suspected that the metal layer will not be uniform and oxygen might penetrate down to the NW. Ti is very reactive with oxygen, so it is difficult to ventilate the sample without compromising it. It was therefore tried to wait 20 minutes in between each metallization, and though this proved to have some effect at the edges of the sample bubbling was still prominent in the middle of the sample where the contacts were. Because of these problems some samples were sent to IBM Zurich where metallization was very good.

To overcome the metallization problem in NTNU nanolab it is believed that loading the sample into the load lock in between each metallization and ventilate the chamber will resolve the heating problem. However since the sample can not be exposed to oxygen it is thought that flusing the sample with N_2 in vacuum will help to cool the sample. This requires higly stable vacuum lines which are not yet installed, and will therefore not be investigated further in this thesis.

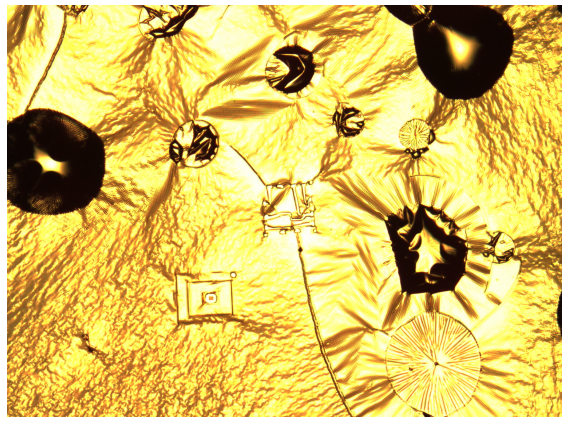

(a)

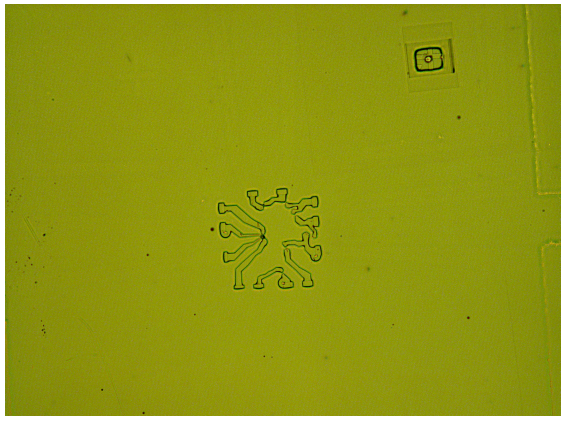

(b)

Figure 4.5: a) Metallization where reisist has bubbled due to heating. b) Metallization without bubbling.

4.2.2 Measurements; SC50 and SC96

Some of the samples from the previos project was measured again before the annealing process to check if they were not degraded over time. They showed the same I-V characteristics as before. Not comletetly ohmic but still with pretty symmetric I-V charcteristics. A new sample with the exact same growth parameters, SC-96 was also tested. This showed excatly the same I-V characteristics as expected. The results can be seen in figure 4.6.

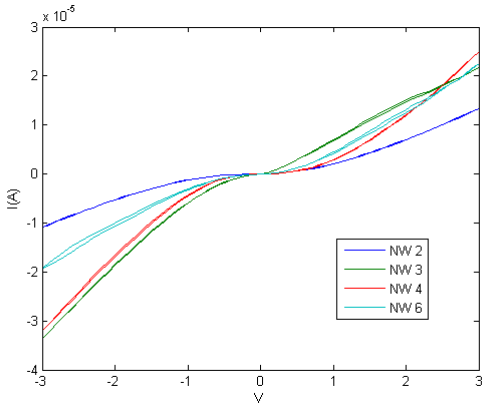

Figure 4.6: I-V characteristics, SC50-5 before annealing.

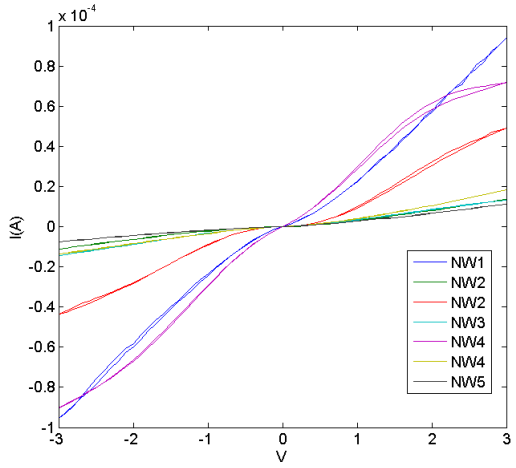

Figure 4.7: I-V characteristics, SC96-1 before annealing.

4.2.3 Annealing; SC50 and SC96

Previous annealing experiments show that annealing gives a slight increase in current, however results show that for annealing at 350 °C the I-V characteristics are very inconsistent and exhibits a low current, which may indicate that the NW itself is damaged. This is suggested for n-type GaAs NWs[9]. This was tried on NWs that had already been annealed 2 times so to check if the NWs could have been damaged due to thermal stress of several annealing, another sample of SC50 which had not been annealed was tested at 400 °C. This showed much better I-V chacteristics with an increase in current and more linear I-V characteristics which for

some NWs were comletely ohmic. This is believed to be due to the formation of the amorpous layer at the SC/metal interface, which enhance ohmic contact by letting carriers flow more freely thorugh the amorphous layer. Pt contacts to GaAs have reported to show this sort of behavior[10]. A comparison of two NWs can be seen in figure 4.9 a) and I-V characteristics of all NWs can be found in the apppendix. To make sure that this sample looked OK, it was examined with SEM and did not show any signs of damage. However as there were no SEM image to compare it to another sample (SC96) was made to check SEM pictures before and after annealing These images showed that it did not look that the NW was damaged, but there was a crack around the metal layer for all of the images. However this should not affect the contact to any extent. This crack was observed both for SC50 and SC96, and does not seem to affect the NW itself as no defects could be seen in the NW. The NW neds are still completely covered by the contact. Resulting I-V characteristics with linearity and high current also indicate that the contact has not been compromised. It can be seen that for SC96-1 the current is lower after annealing. The reason for this may be that the RTP was recalibrated between the annealing of SC50 and SC96. It is therefore possible that the temperature at SC50 actually was a little lower than it was when annealing SC96, and that this slightly higher temperature have degraded the electrical properties of the contacts slightly. Another SC50 sample was also tested at 360° C to check if this temperature was sufficient for making ohmic contact. This was SC50-15 which previously was subject to bad metallization which caused it to have unsymmetric behaviour. As can be seen in figure 4.8 the annealing at 360 ° C had a positive effect on the sample which showed a little better linearity and higher current after annealing, which is consistent with the results achieved from annealing at 320 ° C and 400 ° C, where this sample lies somewhere in between in which improved characteristics are concerned. These results indicate that the doping concentration in these samples was to low to achieve ohmic contact with linear I-V characteristics without the process step of annealing. This subsequently led us to fabricate contacts for a higher doped sample (SC90) for further measurements.

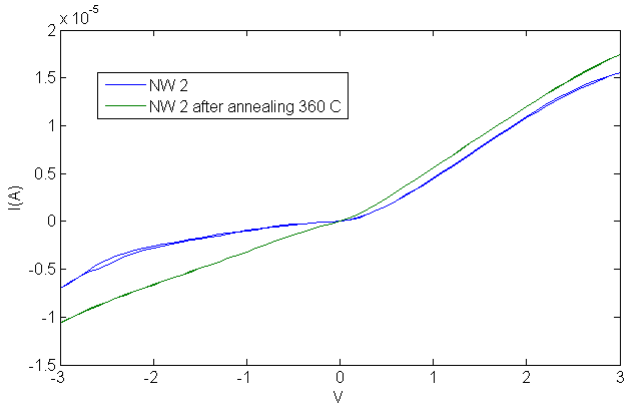

Figure 4.8: I-V characteristics, SC50-15 annealing comparison 360° C.

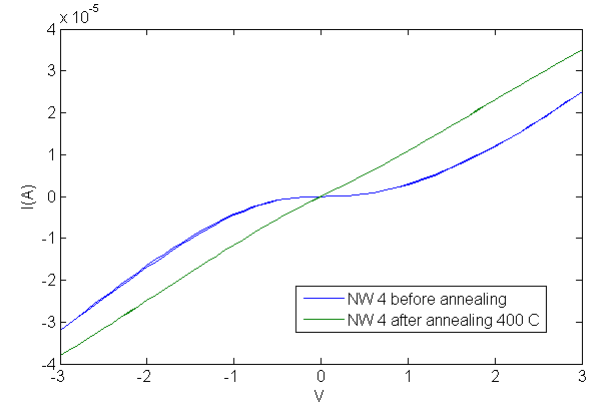

(a)

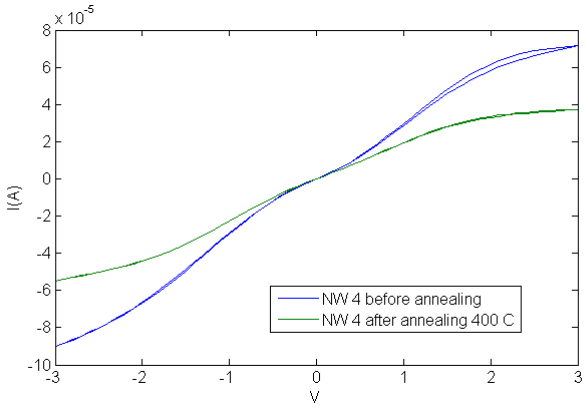

(b)

Figure 4.9: I-V cahracteristics of: a) NW 4 SC50-5 annealing comparison 400° C. b) NW 4 SC96-1 after annealing comparison 400° C.

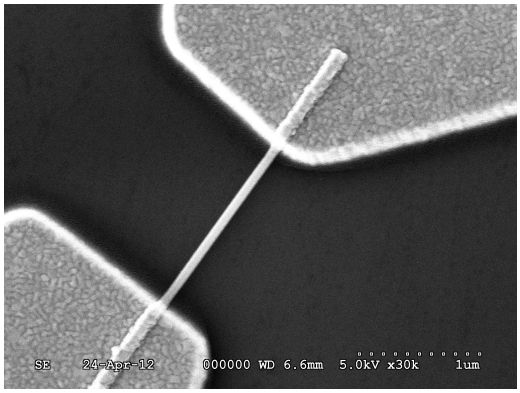

(a)

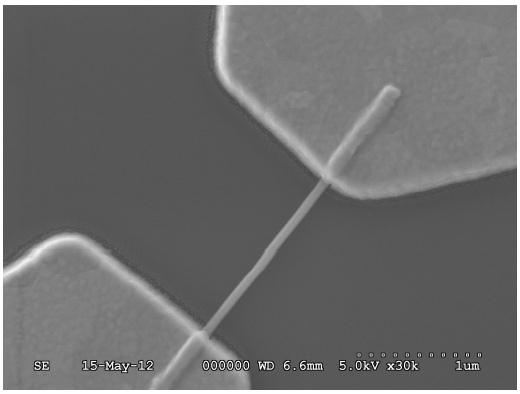

(b)

Figure 4.10: SEM images of: a) SC96 before annealing. b) SC96 after annealing 400 C.

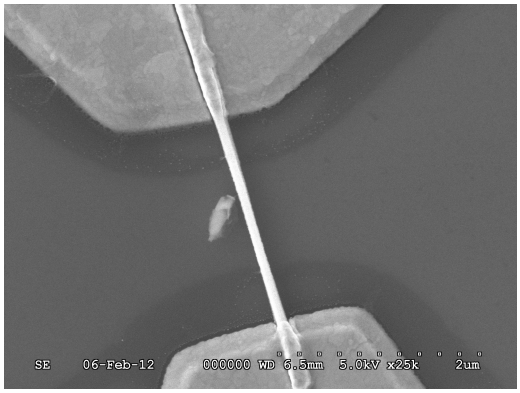

Figure 4.11: SEM image of SC50 after annealing 400 C.

4.2.4 4 probe measurements; SC96

2 NWs for SC96 were measured. The results can be seen in table 4.3. the resistance and contact resitance varied a little bit. Especially NW 2 shows a contact resistance of only 12 percent of the total resistance, which is low. However this variation in contact resistance can be due to fluctuation in fabrication parameters as well as the doping of the NW itself. 4-probe measurements of SC50 showed a contact resistance of 20-30 percent so these results are consistent. As can be seen from figure 4.12 the 4-probe I-V characterstics for both NWs are very linear which means the resistance is constant.

Sample	2-probe	4-probe	Contact	CR percentage
SC96-1 NW 2	60kΩ	53kΩ	7kΩ	12
SC96-1 NW 4	42kΩ	31kΩ	11kΩ	26

Table 4.3: Contact resistance for Ga-assisted GaAs NWs with an expected doping concentration of $3 * 10^{18} cm^{-3}$.

The resistivity and carrier concentration in the NWs were calculated by using equations 2.3 and 2.4. From SEM images of the NWs the mid-electrode distance(L) and diameter(d) for both NWs were measured. For NW 2 the measurements were L= 1,2μm and d = 100nm. For NW 4 the measurements were L = 1,4μm and d = 100nm. A maximum hole mobility of 400 cm^2/Vs was assumed for both cases leading to the carrier concentration found in table 4.4. However a hole mobility of 400 cm^2/Vs is very optimistic, and experiments has shown that this value is almost never achieved. Therefore this estimated carrier concentration has to be considered as an absolute minimum. It is also interesting to assume maximum carrier concentration (expected concentration for thin film for the same growth parameters) which is $3 * 10^{18} cm^{-3}$ for SC96. The hole mobility can then be calculated to see if this is more reasonable(table 4.5). The real value for these to parameters will lie somewhere in between these max and min values.

	NW 2	NW 4
ρ	$346 \bullet 10^{-4} \Omega cm$	$174 \bullet 10^{-4} \Omega cm$
n_h	$0.45 \bullet 10^{18} cm^{-3}$	$0.9 \bullet 10^{18} cm^{-3}$

Table 4.4: Resistivity and minimum carrier concentration of two selected SC96-1 NWs with an assumed maximum hole mobility of 400.

	NW 2	NW 4
ρ	$346 \bullet 10^{-4} \Omega cm$	$174 \bullet 10^{-4} \Omega cm$
μ_h	60 cm^2/Vs	119 cm^2/Vs

Table 4.5: Resistivity and minimum hole mobility of two selected SC96-1 NWs with an assumed maximum carrier concentration of $3 * 10^{18} cm^{-3}$.

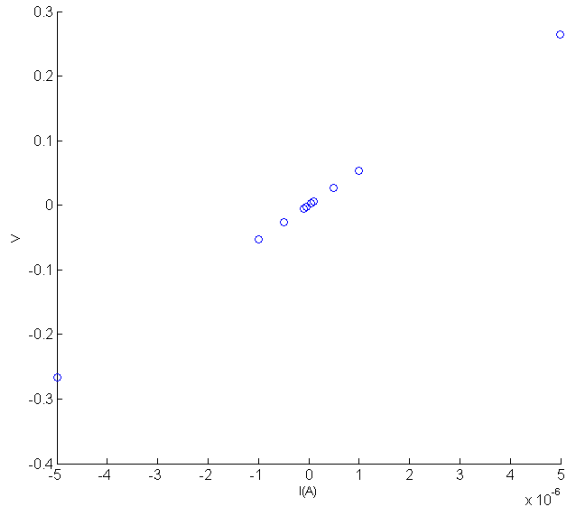

(a)

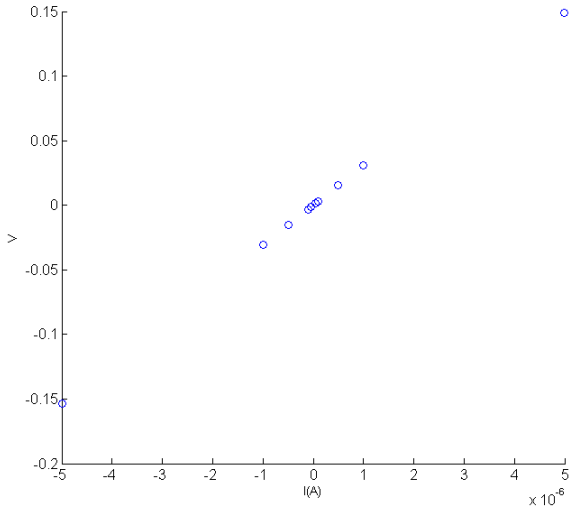

(b)

Figure 4.12: I-V scatter plots of measured voltages for several applied bias currents. a) SC96 NW 2, shows a resistance of 53kΩ. b) SC96 NW 4, shiws a resistance of 31kΩ.

4.2.5 Measurements; SC90

As SC90 is grown with a higher source temperature (1025°C) than SC50 and SC 96(990°C) it is expected that more dopants are introduced to the NWs and thereby increasing doping concentration and current. SC90 was processed in the excactly the same way as SC50. When measured this sample showed higher current and also was much more linear than SC50 which was expected due to the higher doping concentration of this sample. When averaged the current is about 50 percent higher than SC50. When comparing fig. 4.13 and fig. 4.6 one can clearly see that SC90 is more linear for lower voltages than SC50, whithin such a vicinity that some of the NWs can be considered ohmic even before annealing(also see fig. 4.18). This is preferable because annealing is a process step that is unwanted if it can be avoided. Though it does not seem to affect or damage the NW it may effect graphene electrode which will be discussed later in this thesis, so if it is possible to achieve ohmic contact without annealing the sample this is preferable for NW-graphene contact. Nevertheless annealing had to be tested for this sample to see if it further improved the I-V characteristics.

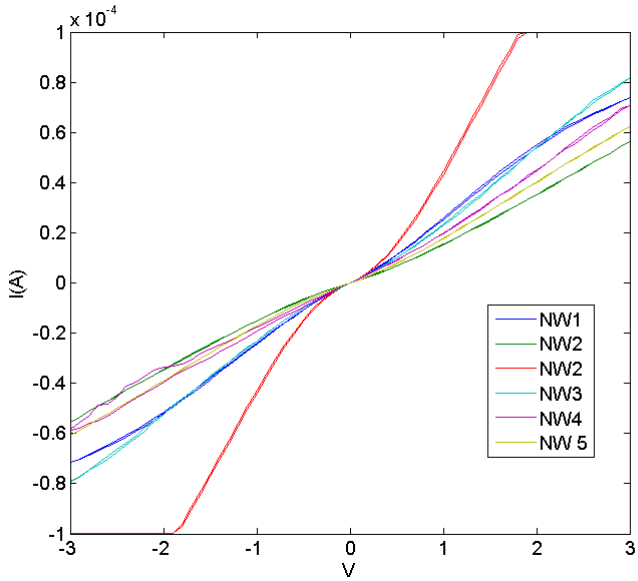

Figure 4.13: I-V characteristcs, highly doped GaAs NWs (SC90-5).

4.2.6 Annealing, SC90

As can be seen from figure 4.14 the annealing show a slight increase in linearity, however the current is slightly lower, as was the case with SC96. The intention of annealing is to enhance the ohmic contact. With SC90 the NWs are already

sufficiently doped to create ohmic-like contact and the annealing does not play a significant role as it did with SC50. Another issue that should be noted is that the crack around the edges of the contacts can be seen in SEM imaging. As this was also observed for SC50-5 which showed great improvement after annealing, this is not believed to have any effect on the NW contact as the NW itself does not look damaged and is still fully covered by the contact.

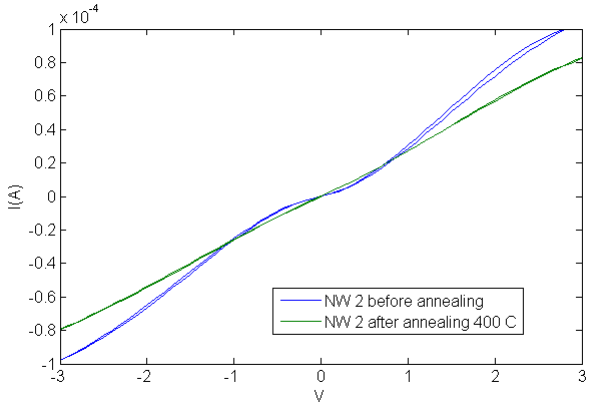

Figure 4.14: SC90 NW 2 annealing comparison.

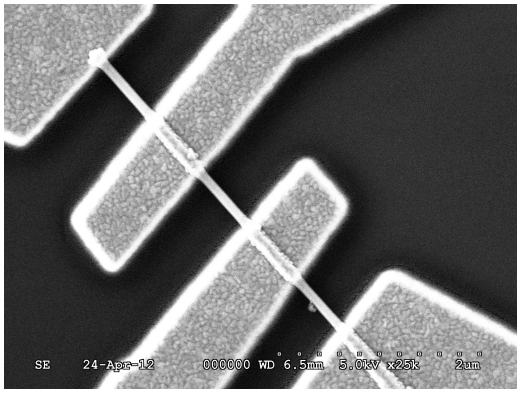

(a)

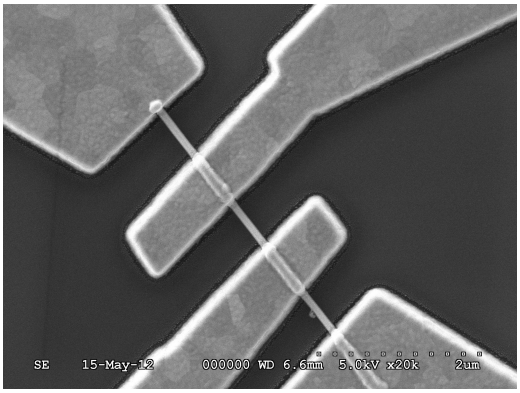

(b)

Figure 4.15: SEM images. a) SC90 NW 2 before annealing. b) SC90 NW 2 after annealing 400 C.

4.2.7 4 probe measurements SC90

1 NW was available for 4-probe measurements. The measurements of SC90 show lower resistivity than SC96 and SC50, which is also expected due to the high current measured for these samples. However when comparing the 2-probe and 4-probe resistance it is clear that the percentage of the resistance which is due to the contact is about the same as for SC50, which again is consistent.

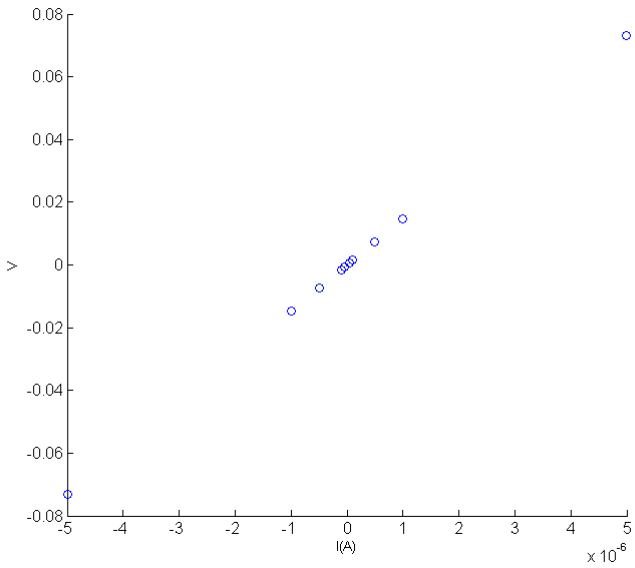

Figure 4.16: I-V characteristics for different bias currents (SC90 NW 2).

Sample	2-probe	4-probe	Contact	CR percentage
SC90-5 NW 4	18kΩ	14,5 kΩ	3,5kΩ	20

Table 4.6: Contact resistance for Ga-assisted NWs with an assumed doping concentration of $1 * 10^{19} cm^{-3}$.

Resistivity was also here calculated for the NW measured. The length of the NW was measured to be 1.4 μm mid electrode-distance and the diameter was measured to be 110 nm. As can be seen from the tables, the estimated carrier concentration here was much larger than for SC50 and SC96, which was to be expected due to the increased doping during growth. This also meant the assumption made that higher NW doping is needed to make contacs ohmic without annealing was correct. Here also the maximum carrier concentration ($1 * 10^{19} cm^{-3}$) was assumed to estimate the minimum hole mobility, which again is consistent with SC96.

	NW 2
ρ	$98 \bullet 10^{-4} \Omega cm$
n_h	$1.59 \bullet 10^{18} cm^{-3}$

Table 4.7: Resistivity and minimum carrier concentration of one SC90-5 NW.

	NW 2
ρ	$98 \bullet 10^{-4} \Omega cm$
mu_h	$63\ cm^2/Vs$

Table 4.8: Resistivity and miminum hole mobility of one SC90-5 NW.

4.2.8 Measurements, As-589 7

As previously mentioned, problems of doping with Au assisted NWs have been prominent. A new batch was therefore tested. In this new growth the Be effusion cell shutter stayed closed for 5 minutes to let the GaAs nucleate under the Au-droplet to try to prevent Au solidification by Be and sidewall diffusion. The growth temperature was also lowered to 520°C to try to prevent this effect. The new NWs were a little bit longer than the Au-assisted samples measured before. Exactly the same processing parameters were used, but still the I-V characteristics looks as they used to, with many of the NWs showing diode-like I-V characteristics. The ones that do not show diode-like behaviour have lower current than Ga-assisted NWs. They were also unsymmetric and more noisy than Ga-assisted NWs. It seems that problems with Au solidifing when it comes in contact with Be during growth is still an issue. Figure 4.18 shows a comparison of measured current of Au-assisted NWs and Ga-assisted NWs. As can be seen from this figure, Ga-assisted NWs show far better characteristics than Au-assisted. No 4-probe measurements was tried on these samples because the NWs were so short that the implementation of a 4 probe contact proved to be difficult, using the current fabrication parameters. Though it was fabricated the contacts showed either short circuit characterstics, because the contacts has to be so close that they connected, or open circuit, because misalignment caused the contact to miss the NWs. Due to their short length much less misalignment is sustainable.

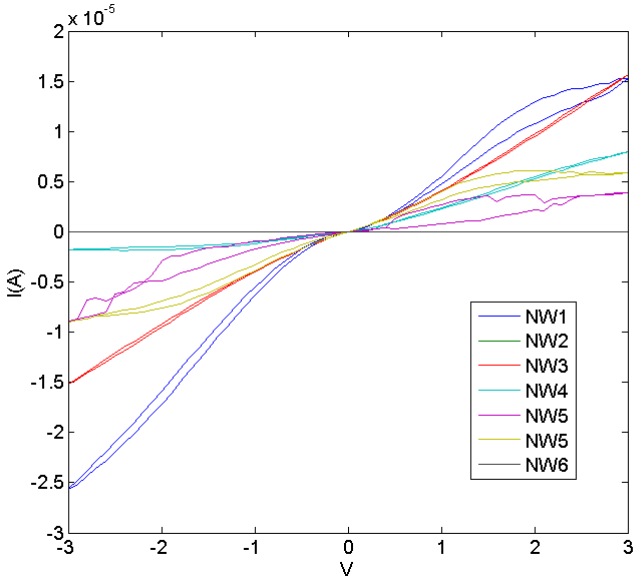

(a)

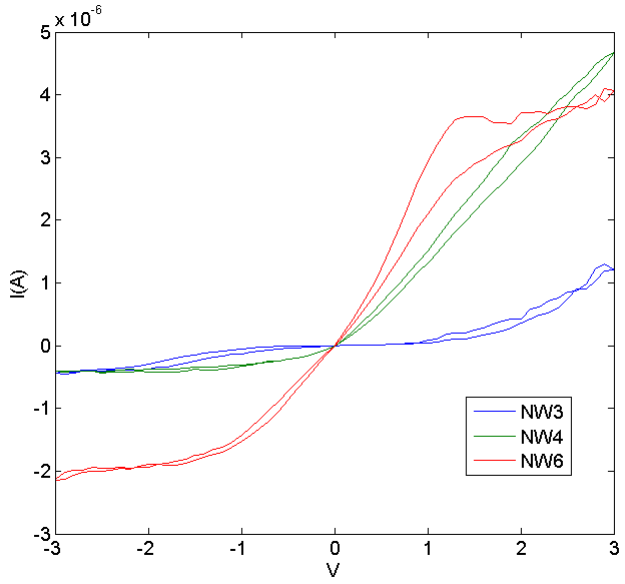

(b)

Figure 4.17: a) I-V characteristics As589-7 1. b) I-V characteristics As589-7 2.

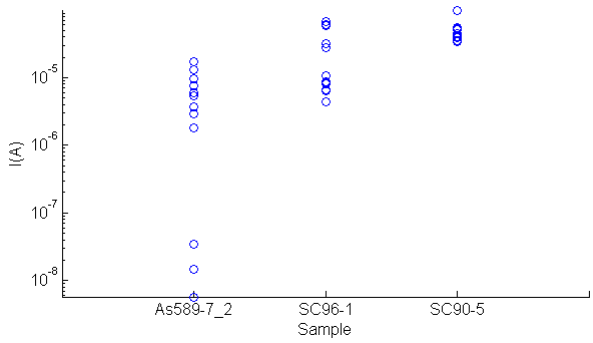

Figure 4.18: Scatter plot of current at 2 V for different NWs.

4.2.9 Annealing, As589-7

These NWs showed no enhancing of linearity or current after being annealed. In fact they seemed to gain worse properties than before annealing. Only 1 NW was measured for 400°C because the sample (As589-7 2) had been comprimised during processing so that only 1 NW remained. The NW that was measured showed open current, and the temperature was therefore lowered to 380°C for As589-7 2. Here all the NWs were measurable, but all NWs showed diode-like current where the current magnitude was lower than before annealing. This may indicate that these NWs which are grown by Au-assisted method are less resistive to heat as they are compromised during growth, because diffusion through the catalyst droplet is difficult. As can be seen from the SEM images (figure 4.20) the NW is looks intact, however it looks to be maybe a little thinner near the left electrode which may indicate that the NWs have been damaged slightly during the annealing process.

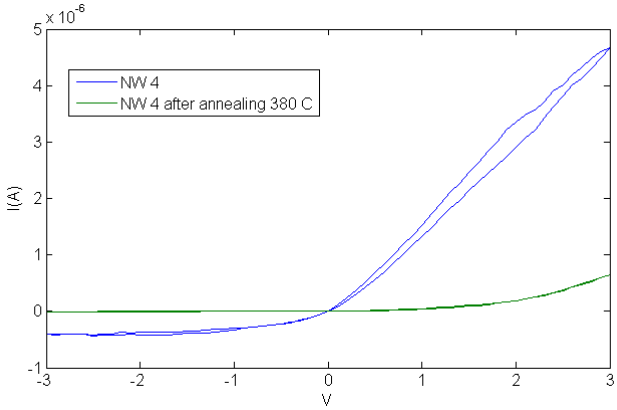

Figure 4.19: As589-7 2 annealing comparison 380° C.

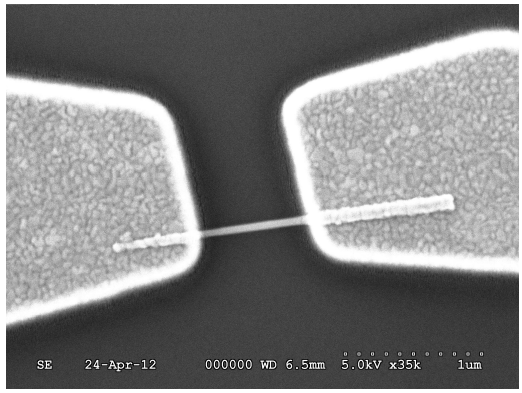

(a)

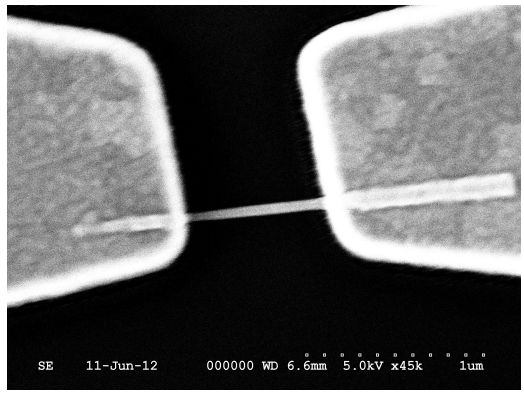

(b)

Figure 4.20: As589-7 2. a) NW 4 before annealing. b) NW 4 after annealing.

4.3 Graphene NW contact

4.3.1 Processing

Several different processing methods were tested. The method carried out in Korea in which the graphene was selecticely transferred to the substrate holds some advantages over the method performed in the NTNU nanolab. Firstly the mechanical exfoliation of kish graphite yields higher quality and more crystalline graphene then CVD-grown graphene. Secondly the advantages of having small strips that can be selecticvely placed is that one is sure to have graphene on a relevant position. However for this method another step is to make contacts to the graphene as well at least as long as this does not cover the prefabricated electrodes already. The method tested in NTNU nanolab also has the disadvantage that it has a lot of processing steps like etching and cleansing. This causes the chance of degrad-

ing the sample to increase. For instance it is more likely to wrinkle because the PMMA is not completely rigid, but it is soft baked so that it is easily removable. Also residues of resist is another issue with this method. There is also the issue of using a negative resist, which is difficult to completely remove. The resist is an insulator so it should not have anything to say regarding the electrical conductivity between graphene and GaAs but it makes it impossible to further process the sample. Though this method has some disadvantages it is an easy way of transferring graphene without the need to precisely place it. The graphene would cover large areas which can easily be trimmed using the EBL and plasma cleanser, and there is no need to make seperate contacts to the graphene beacuse they already covers predeposited electrodes.

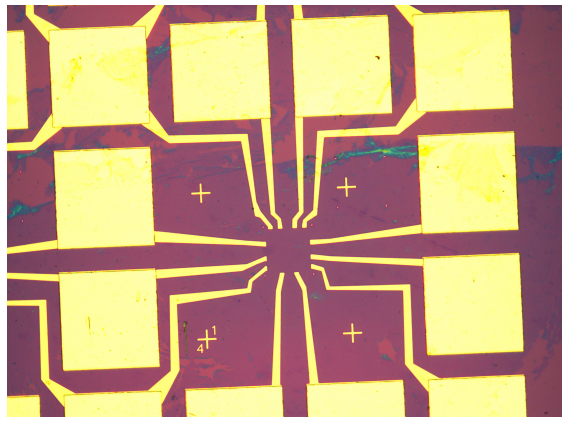

(a)

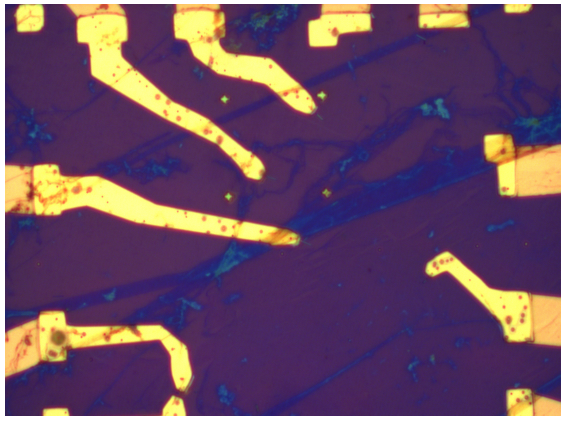

(b)

Figure 4.21: a) Image of sucessful GP transfer. b) GP transfer to NW position. Same sample as image a, but with residues from PMMA on top.

In the process itself it turned out that the method deviced in Korea was unusable

when appliyng contacts with the evaporator in NTNU. Because the resist started to bubble this caused the graphene to be wrinkle and crack on the substrate. After metallization it was concluded that the graphene had vansihed from the sample. No graphene could be seen in the optical microscope which was confirmed when measurements showed open current.

The process used in NTNU nanolab went ok, without any significant problems and is a good way of making NW/graphene contacts for characterization and analysis. However since the graphene sheets are not selctively placed the chance is fairly small that a graphene sheet will be deposited on a relevant substrate position. In the attempts made at NTNU only 1 in 5 transfers went succesfully, so it is not a very reliable method for graphene transfer. It is believed that this is caused because the graphene on the Cu foil is not continous. The reason this is believed is because that the 1 succesful transfer several large sheets were succesfully tranferred to the substrate, while for the 4 unsuccessful transfers the graphene was much more fragmented. Images of these transfers can be found in the appendix. However, once the graphene has been succesfully transfered the only problem with this method is that it usually leaves some sort of residue on the surface which makes it hard to precisely characterize the structure of the contacts through microscopes.

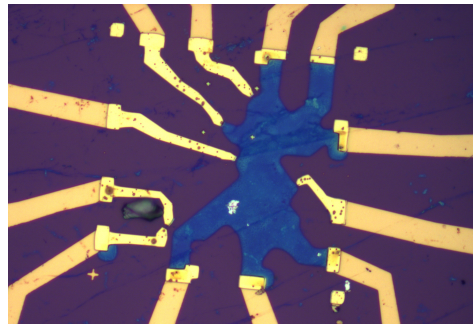

Figure 4.22: SC90-3 after resist removal and O_2 plasma trimming of the graphene.

4.3.2 Measurements

Initial measurements of 2 NWs show that the contact between NWs and graphene is completely ohmic, with a current of about 30 uA at 3 V. This is expected due to the fact that graphene which is exposed to air is expected to be p-type. A p-type/p-type contact is expected to be ohmic. However the processing of this first sample was subject to experimental processing because this was the first sample made. For instance a lot of residues can be seen on the sample after the graphene etching. Some misalignment can be seen for the last processing step which may cause the graphene and metal electrode to be in contact. In addition the ashing of the graphene had to be increased in time to etch away the graphene that shorted the NW electrode. However an interesting point is that only two of the NWs show a current of 30 uA at 3 V whilst the other NWs on this sample showed a current

of about 100 uA at 3 V which is surely a short circuit. This also coincides with the images where the 2 NWs showing the low current definitely have a gap between the NW electrode and graphene. The other NWs have electrodes that are so close to the graphene that it is difficult to see form the image if they get shorted or not.

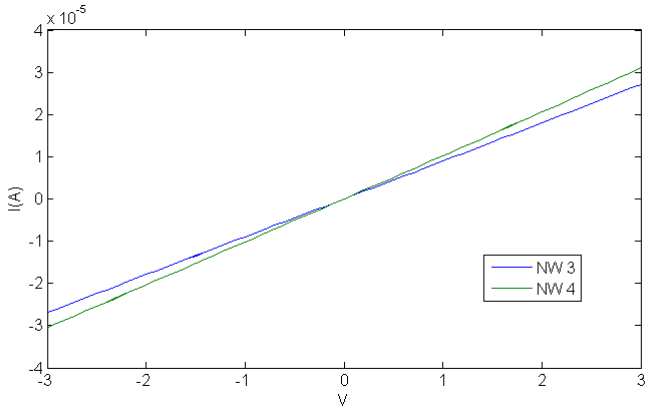

Figure 4.23: I-V characteristics SC90-3 with GP electrode.

4.3.3 SEM of graphene contacts after measurment

Because SEM imgaing itself might deposite carbon at the imaging spot, these images had to be taken after the electrical meausurments to be sure there was no carbonic residues at the surface of the sample. SEM imaging taken of the NW/graphene contacts after measurements show that the NWs themselves are damaged. This can be seen in figure 4.23. It is therefore difficult to determine what is measured. However earlier experiments tells that samples with the same kind of damage could have been measurable. One possible reason why the NWs have been damaged is due to the fact that it is etched several times by HCl during the fabrication process which is designed to remove oxide. If the NW is exposed to much to HCl it might become damaged. The sample with NW/graphene contact was subjected to a lot of processing steps, some of which were carried out multiple times because this sample was the first sample and therfore had to go through various testing. However the graphene edge can be seen, and it is quite clear that the graphene-trimming process has been successfull. This indicates that there should be no short-circuit between graphene and electrode which further indicates that the NWs themselves are measurable. However it can not be ruled out that the current generated between the electrode and graphene could be generated due to external factors which have not been examined during the cause of these experiments. It is therefore impossible to conclude that this behaviour is real NW/graphene contact behaviour, but the knowledge available at this time suggests that it is.

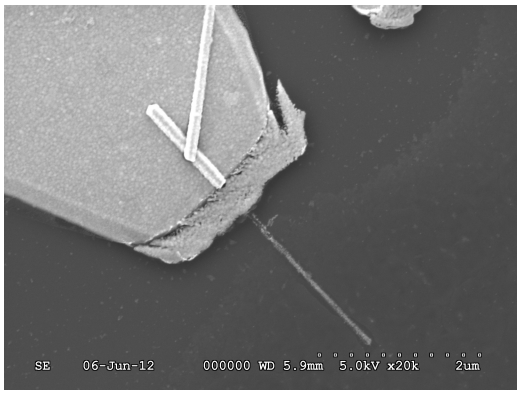

Figure 4.24: SEM image showing the damage on NW 4 after processing.

4.3.4 Gate-dependence measurements

The first gate-dependence measurements was done on the NW/graphene sample (SC90-3). Initial measurements were done solely on graphene, and these I-V curves show that gate current is in the range of pA which indicates that the sample does not leak through the back-gate (figure 4.25), however the current shows a slight increase at around 25 V. This will be discussed later in this section. It can also be seen that Ids is very noisy but it can be seen that the trend is as expected. Graphene which is exposed to air is usually p-doped Therefore this will show an increase of resistance (decrease of current) near the Dirac point. It can therefore be concluded that we are measuring on single or few-layer grahene.

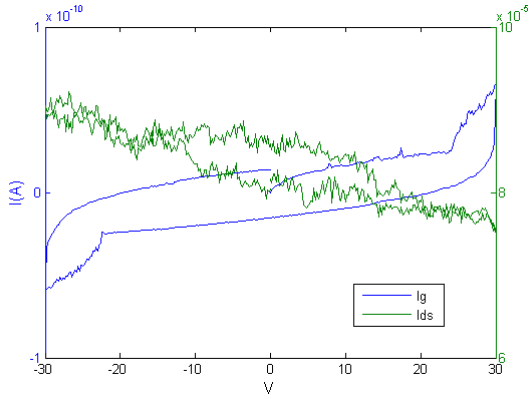

Figure 4.25: Graphene gate-dependence measurements (SC90-3). Vds = 1 V.

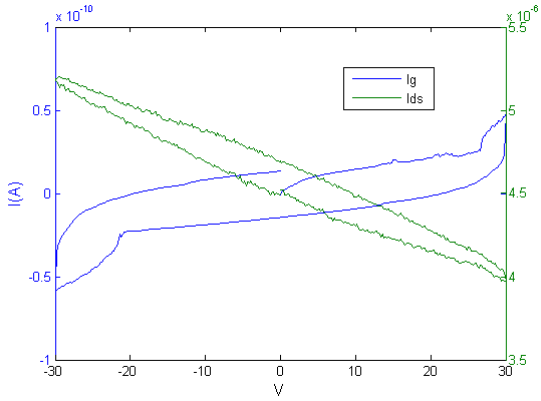

(a)

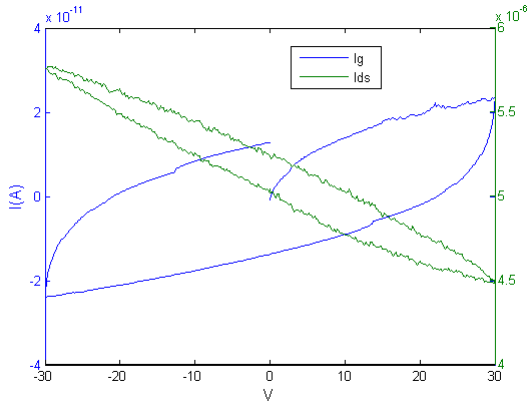

(b)

Figure 4.26: a) Gate-dependence measurement graphene/NW3 contact(SC90-3). b) Gate-dependance measurement graphene/NW4 contact(SC90-3). Vds = 1 V

The other sample(SC90-5) was measured for a voltage sweep of 30, 40, 50 and 60 V. This showed a current drop of about 3 times the maximum current value (30 μA - 10 μA) which corresponds to already measuring results[26], again proving that the graphene is measurable. Ids measurements showed that there was a change at around 40 V that suggests carrier concentration in the graphene changes from p-type to n-type. However it can be seen that there is a spike in gate current at the same position, which is uncertain wether is a cause or effects of the change in Ids. To further test this, there is a need to make the gate contact on top of the graphene, in stead of the setup which was measured in this thesis. This again is not possible to do with the e-beam evaporator setup at NTNU due the risk of graphene wrinkling.

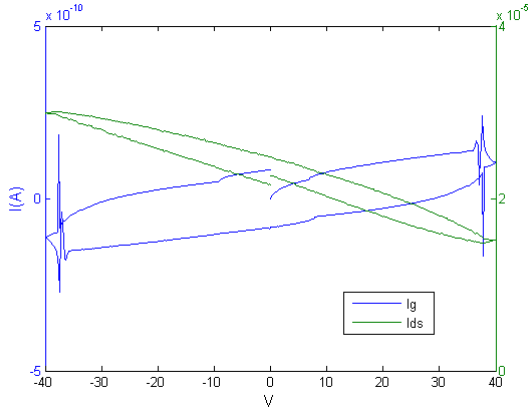

Figure 4.27: Gate-dependence measurement graphene with a 40V sweep (SC90-5). Vds = 100 μV

Chapter 5

Conclusions and Future Work

It can be concluded that the ohmic contact to Be-doped p-type core GaAs NWs was aschieved by annealing at temperatures of 380 - 400°C or by increasing source temperature for higher doping concentration during MBE growth. However ohmic contact is not always achieved and one could see that current magnitude from the same growth conditions, and even from the samme proccesing sample varies quite alot. This is believed to be due to fluctuation of process parameters or inhomogenous doping during growth.

Gold assisted NWs still show very unfavorable I-V characteristics in ohmic-contact sense. Even though new samples were tested.with a different growth scheme, it seemed like the NWs still suffered from lack of incorporation of dopants.

Two ways of transferring graphene to NW substrate was processed. The print-transfer method was superior in the sense that it could selectively place a high quality graphene sheet on desirable sustrate locations. However this method creates the need for a final metallization step, with the graphene on the substrate. As graphene is very fragile this method proved to be unfeasable in our e-beam evaporator as the heating from the evaporator caused the resist to bubble and therefore wrinkle and/or remove the graphene entirely from the substrate. The second method was using CVD grown graphene on Cu foil, which did not depend on a final metallization step. However as graphene was not placed selectively, NW/graphene contact was hard to achieve.

Graphene/NW contact were established where initial results showed the contact to be completely ohmic. However due to the damaging of the NWs confirmed by SEM imaging, these results have yet to be verified.

Further work should include further establishment of the NW/graphene contact, both in terms of the processing itself, to create a highly reliable measure of con-

tacting NWs to graphene, and in terms of establishing the nature of the electrical properties of such a contact. Though initial measurements indicated that this type of contact could be comletely ohmic, it needs to be further investigated. In addition optical measurements should be carried out, as graphene is optically tranparent this will give a more correct measurement of photocurrent in the NW as the electrode itself does not interfere with the illuminated light, and charge carriers can form uniforlmy throughout the length of the NW.

Further work should also be commited to investigate contacts to n-type GaAs core NWs and p-type core/n-type shell NWs. Ohmic contact needs to be established for these types of NWs as well if a functional radial or londitudinal p-n junction NW is to be a efficient as the integral part of a solar cell device.

Bibliography

[1] Fabrication and Characterization of Ohmic Contacts to P-Type Self-Catalyzed GaAs Nanowires
Ole M. Christoffersen, Project Report, NTNU, 2011

[2] Gallium Arsenide Materials, Devices, and Circuits
M.J. Howes and D.V. Morgan, ISBN: 0 471 90048 6 (1985)

[3] Favriaction of GaAs Devices
Albert G. Baca and Carol I.H. Ashby, Emis Processing Series 6

[4] Fabrication and Characterization of Single GaAs Nanowire Devices
Åsmund Bakke Bø, Master Thesis, Norwegian University of Science and Technology(2010)

[5] Growth and structural characterization of III-V nanowires grown by molecular beam epitaxy
Dheeraj Dasa, Doctoral Thesis,Norwegian University of Science and Technology(2010)

[6] Low Resistance Pd/Zn/Pd Au Ohmic Contacts to P-type GaAs
R. Bruce, D. Clark and S. Eicher, Journal of Electronic Materials, Vol 19, No. 3, 225 - 229 (1990)

[7] High yield of self-catalyzed GaAs nanowire arrays grown on silicon via gallium droplet positioning
S. Plissard, G. Larrieu, X. Wallart and P. Caroff, Nanotechnology 22 1-7 (2011)

[8] Low Level Measurements Handbook, 6th edition
Keithley Instrumenst, Inc. Cleveland Ohio(2004)

[9] Ohmic contact to n-GaAs nanowires
C. Gutsche et al, Journal of applied physics 110, 014305 (2011)

[10] Amorphous phase formation and initial inerfacial reactions in the platinum/-GaAs system
Dae-Hong Ko and Robert Sinclair, Journal of applied physics 72 (5) 2036 - 2042 (1992)

[11] The Au-Be(Gold-Beryllium) System
R.P. Elliot and F.A. Shunk, Bulletin of Alloy Phase Diagrams Vol.2 No.4 478-479 (1982)

[12] Theoretical analysis and modeling of light trapping in high efficiency GaAs nanowire array solar cells
Wen et al. Applied physics letters 99, 143116 (2011)

[13] Nanowire solar cells
Garnett et al. Annual review of materials research 41:11.1-11.27 (2011)

[14] STM studies of Fermi-level pinning on the GaAs(001) surface
M. D. Pashley and G. P. Srivastava, Phil. Trans. R. Soc. Lond. A 1993 344, 533-543

[15] Electric Field Effect in Atomically Thin Carbon Films
A.K. Geim, K.S. Novoselov et. al, Science 306, 666 (2008)

[16] Optical properties of graphene
L.A. Falkovsky, Journal of physics: Conference Series 129 (2008) 012004

[17] Creation of nanostructures with poly(methyl methacrylate)-mediated nanotransfer printing
L. Jiao et al. J. Am. Cem. Soc., 130(38), 12612 (2008)

[18] http://www.ioffe.ru/SVA/NSM/Semicond

[19] http://www.springermaterials.com/

[20] http://serc.carleton.edu/research_education/geochemsheets/techniques/SEM.html

[21] http://www4.nau.edu/microanalysis/Microprobe-SEM/Signals.html

[22] Optical properties of heavily doped GaAs nanowires and electroluminescent nanowire structures
A Lysiv et al. Nanotechnology 22 (2011) 085702 1-8

[23] P-Doping mechanisms in catalyst-free Gallium Arsenide nanowires
J. Dufouleur et al. Nanoletters, DOI: 10.1021/nl100157w

[24] Toward clean and crackless transfer of graphene
X. Liang et al. ACS Nano, Vol.5, No.11, 9144-9153 (2011)

[25] Wafer-scale synthesis and transfer of graphene films
Y. Lee et al. Nanoletters 10, 490-493 (2010)

[26] Fine structure constant defines visual transparency of graphene
A.K. Geim, K.S. Novoselov et al. Science Vol 320, (2008)

Appendix A

Other measured I-V characteristcs

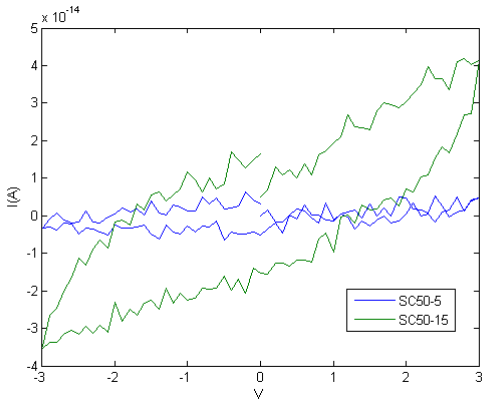

Figure A.1: Gate leakage measurements of SC50-5 and SC50-15 to make sure no current was leaking through the backgate. It can be seen from the figure that the current is so small it is only due to surface tension and fluctuating carriers. This is also the trend that can be seen when measuring open current I-V measurements with only air between probes.

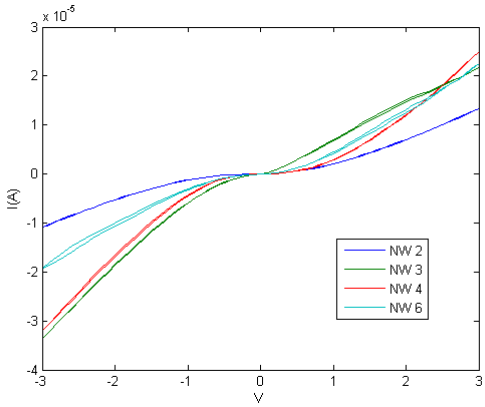

(a)

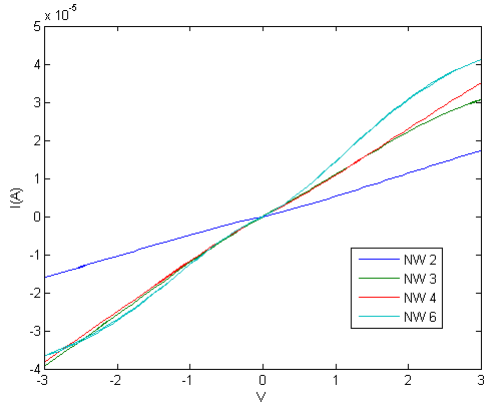

(b)

Figure A.2: a) SC50-5 before annealing. b) SC50-5 after annealing 400 C.

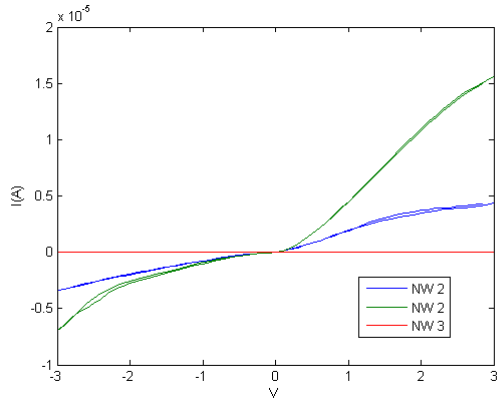

(a)

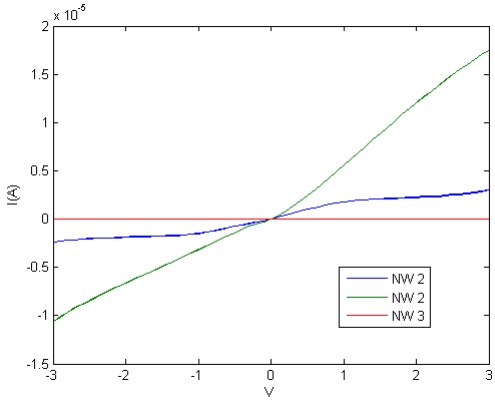

(b)

Figure A.3: a) SC50-15 before annealing. b) SC50-15 after annealing 360 C.

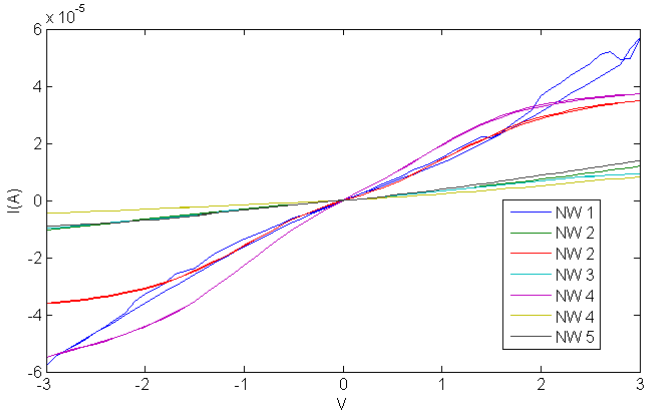

Figure A.4: SC96-1 after annealing 400 C.

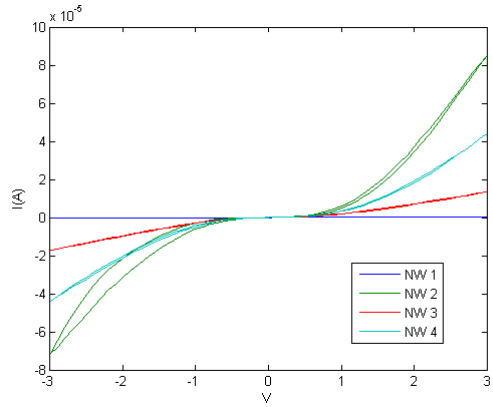

(a)

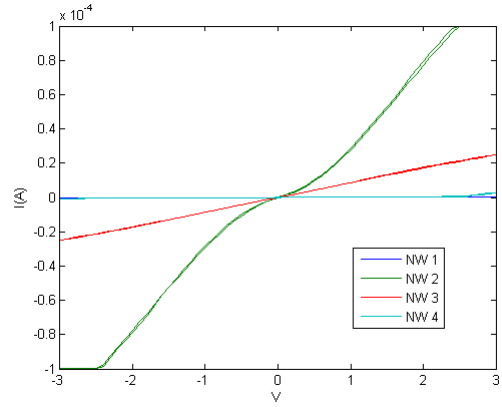

(b)

Figure A.5: a) SC90-1 before annealing. b) SC90-1 after annealing 400 C.

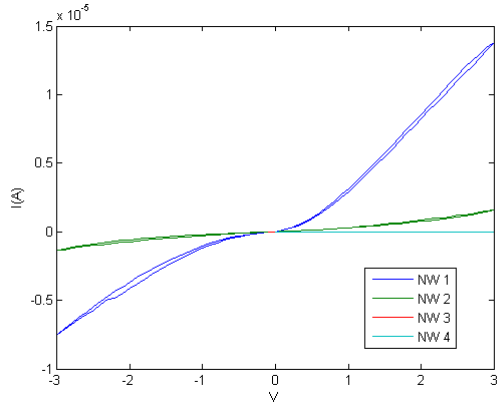

(a)

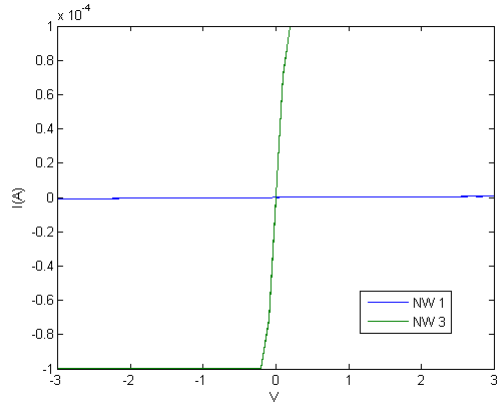

(b)

Figure A.6: a) SC90-2 before annealing. b) SC90-2 after annealing 400 C.

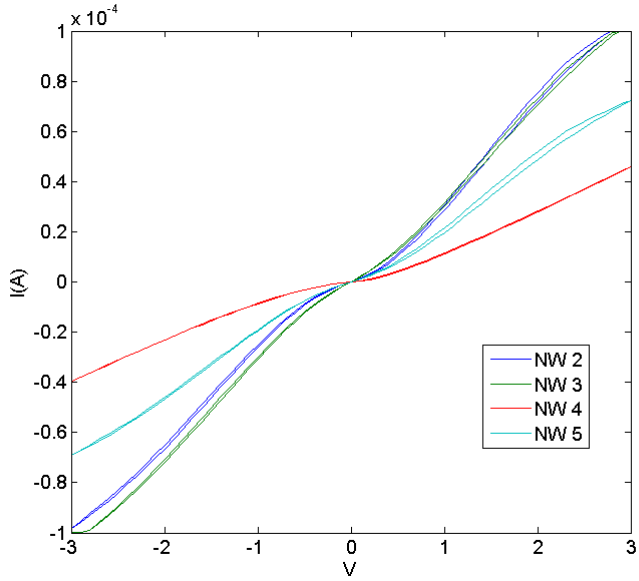

(a)

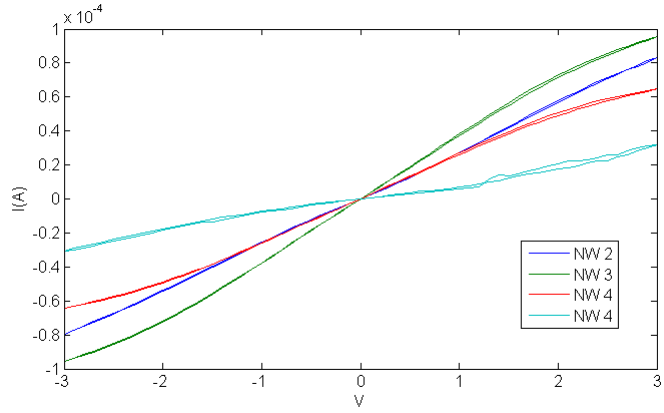

(b)

Figure A.7: a) SC90-6 before annealing. b) SC90-6 after annealing 400 C.

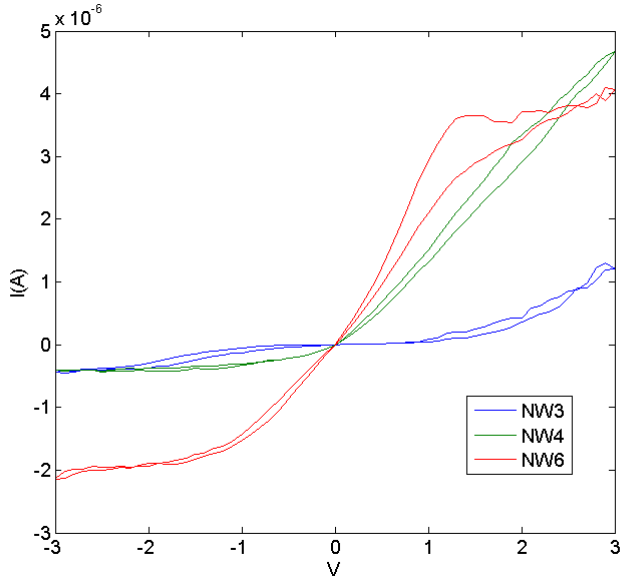

(a)

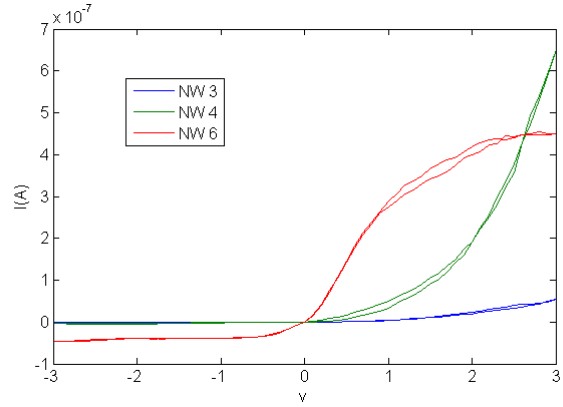

(b)

Figure A.8: a) As589-7 2 before annealing. b) As589-7 2 after annealing 380 C.

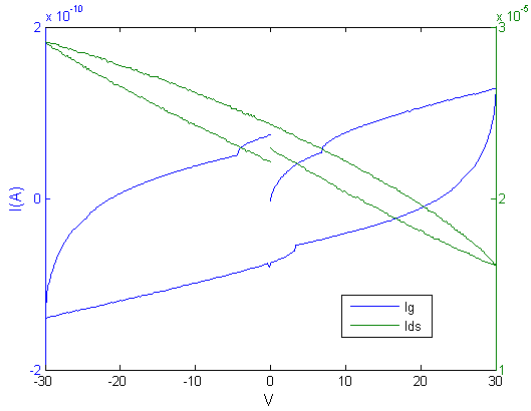

(a)

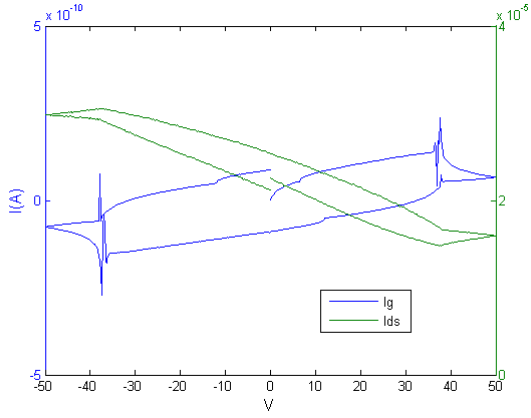

(b)

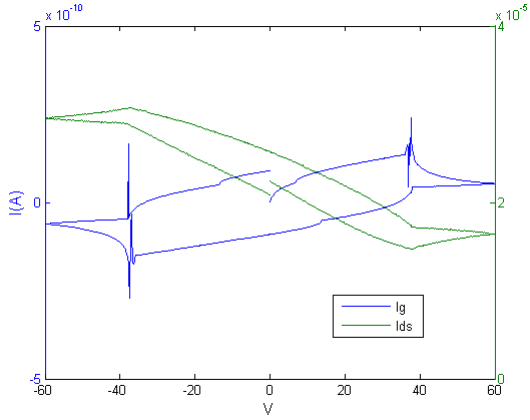

(c)

Figure A.9: Gate-dependance measurements of SC90-5. a) 30 V b) 50 V c) 60 V.

Appendix B

Other images

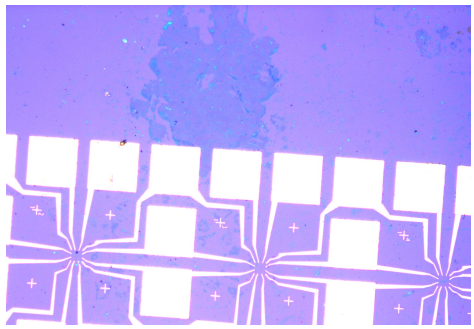

(a)

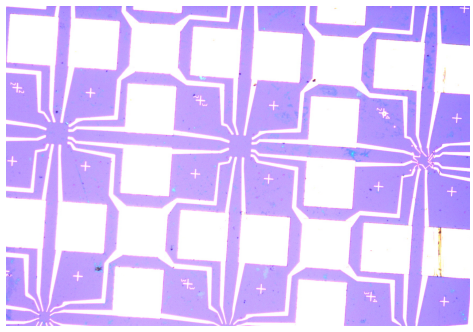

(b)

Figure B.1: Images of unsuccesfull graphene transfers.